A CLIMATE CHANGE REFERENCE ATLAS

WATER RESEARCH COMMISSION

South African Weather Service
ISO 9001 Certified Organisation

2017

Based on CMIP5 – CORDEX downscaling

TABLE OF CONTENT

1.   Introduction

With increased risks posed by global warming and climate change to various climate sensitive sectors, many studies have already been conducted on generating or analysing possible near to far term future projections of likely changes in atmospheric variables. South Africa, which is regarded to be specifically vulnerable to climate change due to its geographical location in the dry sub-tropics and socio-economic landscape, is no exception. On a policy basis, South Africa has already made considerable progress through its Department of Environmental Affairs (DEA) in developing a National Climate Change Response White Paper (DEA, 2011), and is advancing towards putting a National Adaptation Plan (NAP) on the table.

These precautions depend on reliable projections of key impact meteorological variables, like rainfall and temperature, in response to an increase in anthropogenic Greenhouse Gas (GHG) concentrations. The only scientific resources that are capable of generating such projections, are atmospheric models, which are sophisticated computer programmes written to solve the equations of atmospheric flow dynamics and physics. Fundamentally, projections are currently being generated by different Global Climate Models (GCMs) hosted by different research institutions, each with its own formulation of the atmospheric flow dynamics and physics. Significant differences might therefore occur in projection results, which can contribute to uncertainties in what the future might hold. However, when taking an ensemble of such projections into consideration, one might either identify consistent change patterns or larger variability in model outputs. Consistent change patterns might provide more confidence in the likelihood of a projection to occur, while higher variability in model output could lead to greater uncertainty.

Therefore, the larger the number of GCM generated projections, the better the possibility of capturing cross-model output spread and the better the opportunity to address uncertainties in future climate projections.

The purpose of the South African Weather Service (SAWS) Climate Change Reference Atlas is therefore not only to provide a visual platform for viewing various climate projections of rainfall and temperature, but also to add to the number of projections that are already available in South Africa for comparison.

2.   Projection area

The area considered in the atlas extends from 14.96° to 34.40° East, and 35.64° to 20.24° South, which does not only include South Africa, Lesotho and Swaziland, but also the southern parts of Namibia, Botswana, Zimbabwe and Mozambique. In addition, South African province borders were also included to provide a spatial provincial perspective to future climate change projections.

3. Variables and time periods

Future projections of rainfall and near-surface temperature are presented for the two 30-year periods extending from 2036 to 2065 (near future) and 2066 to 2095 (far future). Projected changes are expressed relative to the historical 30-year period of 1976 to 2005. Daily model simulated values of rainfall totals and temperature averages are used to generate projections of annual change, as well as projections of 3-month seasonal change. The seasons considered are December-January-February (DJF), March-April-May (MAM), June-July-August (JJA) and September-October-November (SON). For both variables, projections are expressed in terms of change of the median, change of the 10% percentile (change in the lower spectrum of values) and change of the 90% percentile (change in the higher spectrum of values). I addition, rainfall total change are also expressed as percentage (%) change relative to the historical period.

4. GHG concentration pathways

Four Representative Concentration Pathways (RCPs) have been considered in the fifth Assessment Report (AR5) (Taylor *et al*., 2012) of the Inter-Governmental Panel on Climate Change (IPCC) (IPCC, 2013). These Greenhouse Gas (GHG) concentration (not emission) trajectories, which are all considered as realistic, were used by modellers as atmospheric system forcing for generating climate response and change projections. The RCPs, namely RCP2.6, RCP4.5, RCP6.0 and RCP8.5, have been defined according to their contribution to atmospheric radiative forcing in the year 2100, relative to pre-industrial values. For example, the addition to Earth's radiation budget as a result of an increase in GHGs are RCP2.6 = +2.6 $W.m^{-2}$, RCP4.5 = +4.5 $W.m^{-2}$, RCP6.0 = +6.0 $W.m^{-2}$ and RCP8.5 = +8.5 $W.m^{-2}$.

For generating climate change projections for South Africa in this atlas, a medium-to-low (RCP4.5) and high (RCP8.5) pathway were selected. The RCP4.5 and RCP8.5 trajectories are associated with CO_2 concentrations of approximately 560 ppm and 950 ppm, respectively, by the year 2100 (Riahl *et al*., 2011). The RCP8.5, also known as "business as usual" are projected to increase even further to a CO_2 concentration ceiling of approximately 1200 ppm after the year 2100, while the RCP4.5 is based on active GHG emission reduction interventions that could lead to a ceiling of approximately 560 ppm (a doubling of concentrations since the start of the industrial revolution) by the year 2100, while concentrations could stabilise or even decrease after the year 2100.

5. Models and downscaling

Results from historically and projected (historically: 1976 to 2005; projected: 2006 to 2095) simulations by nine GCMs (Table 1) were analysed for this atlas. Climate change projection output from all nine GCMs were included in the IPCC AR5 reports. As indicated in Table 1, the spatial resolution of GCM grid squares are relatively coarse,

especially if applied to produce South African provincial scale climate change projections.

Model name	Institute/country	Resolution	Literature
CanESM2m	CCCMa (Canada)	2.8° x 2.8°	Arora et al., (2011)
CNRM-CM5	CNRM-CERFACS(France)	1.4° x 1.4°	Voldoire et al., (2013)
CSIRO-Mk3	CSIRO-QCCCE (Australia)	1.9° x 1.9°	Rotstayn et al., (2013)
IPSL-CM5A-MR	IPSL (France)	1.9° x 3.8°	Hourdin et al., (2013)
MICRO5	AORI-NIES-JAMSTEC (Japan)	1.4° x 1.4°	Watanabe et al., (2011)
HadGEM2-ES	Hadley Centre (UK)	1.8° x 1.2°	Collins et al., (2011)
MPI-ESM-LR	MPI-M (Germany)	1.9° x 1.9°	Ilyina et al., (2013)
NorESMI-M	NCC (Norway)	1.9° x 2.5°	Tjiputra et al., (2013)
GFDL-ESM2M	GFDL (USA)	2.0° x 2.5°	Dunne et al., (2012)

Table 1: Projections from nine Global Climate Models (GCMs) were used for downscaling to a finer spatial resolution (0.4° x 0.4°) using the RCA4 Regional Climate Model (RCM).

To address the spatial scale limitations posed by the GCM fields, dynamical downscaling to a finer spatial resolution (0.44° x 0.44°) was obtained using the Rossby Centre regional model (RCA4), forced across its lateral boundaries by the nine listed GCMs. Nine ensemble member projections were therefore available for calculating ensemble means, and the spread in model output across the nine ensemble members were used in an effort to quantify uncertainty (see Section 7).

The RCA4 is a coupled ocean-atmosphere Regional Climate Model (RCM) based on the Numerical Weather Prediction (NWP) model HARLAM (Undén *et al.*, 2002). The RCA4 simulated projections considered for this atlas formed part of the Coordinated Regional Climate Downscaling Experiment (CORDEX) (Jones *et.al.*, 2011).

6.   Quantification of uncertainty

Climate change projections are based on probable future outcomes, and are therefore associated with uncertainties. In this atlas, uncertainties are assumed to be a result of our understanding of the flow dynamics and physics of the atmosphere, and our ability to formulate these processes in terms of numerical techniques and empirical estimates or physical parameterization in climate models. Globally, climate models are developed by a variety of research groups. Although there is a fair agreement in the formulation of flow dynamics, each one of these groups still follows unique methods in physical parameterizations. This approach could lead to variations in model simulated output, accompanied by uncertainties regarding the performance of models.

Therefore, an important aspect is our common understanding, amongst different model developing groups, of the formulation of physical processes. For example, limited understanding of the physical formulation of an atmospheric process might

result in more diverse answers, which might result in a wider spread of model outcomes. It is therefore assumed that the spread of model outcomes is a reflection of our ability to resolve atmospheric processes, and can therefore be associated with the degree of uncertainty in the model output. The larger the spread, the larger the uncertainty, and the more confined model output, the smaller the uncertainty.

It is known that ensemble averaging of output from a range of climate models might produce a better reflection of reality, in contrast to output from a single model (Giorgi and Mearns, 2002). For a group of N models, the direct (non-weighted) ensemble average of a variable T, which represent the average of differences between the actual and projected values (or residuals), can be calculated by:

$$\overline{\Delta T} = \frac{1}{N} \sum_{i=1}^{N} \Delta T_i$$

where Δ indicate the model simulated change.

The spread in model outcomes amongst the residuals (ΔT_i), may be expressed as the root-mean-square difference (rmsd):

$$\delta_{\Delta T} = \frac{1}{N} \sum_{i=1}^{N} [(\Delta T_i - \overline{\Delta T})^2]^{\frac{1}{2}}$$

The uncertainty range, centred around $\overline{\Delta T}$, is then given by $\pm \delta_{\Delta T}$. Note that if the projection change follows a Gausian Probability Density Function (PDF), $\delta_{\Delta T}$ would be equivalent to the standard deviation and 1 x $\pm \delta_{\Delta T}$ (2 x $\pm \delta_{\Delta T}$) would approximately cover the 68% (95%) confidence interval, or 68% (95%) of the residuals will fall within the 1 x $\pm \delta_{\Delta T}$ (2 x $\pm \delta_{\Delta T}$) range.

For each projection map in this atlas, the associated rmsd map is also provided (blue shading to the right of each projection map). At each map location, this provides valuable information about the uncertainty range ($\pm \delta_{\Delta T}$) of projected model simulated residual values, and also gives a relative perspective of spatial areas associated with higher and lower projection uncertainties.

7. Model verification

Before climate model projections can be used, it is appropriate to first verify the historical model simulations against observations. This is because one can argue that if a model performs well in reflecting observed climate in its historical simulations, the models might also perform well in generating climate projections.

Firstly, historical (1976 to 2005) nine-member ensemble mean RCA4 RCM simulations of average annual total rainfall (mm.year^{-1}) and annual mean temperature (°C) have been compared to the associated observational fields. For observed rainfall, data obtained from the Global Precipitation Climatology Centre (GPCC) (Scheider et al., 2011) were used, while the NOAA GHCN_CAMS Land Temperature Analysis were selected to represent observed temperature (Fan and van den Dool, 2008).
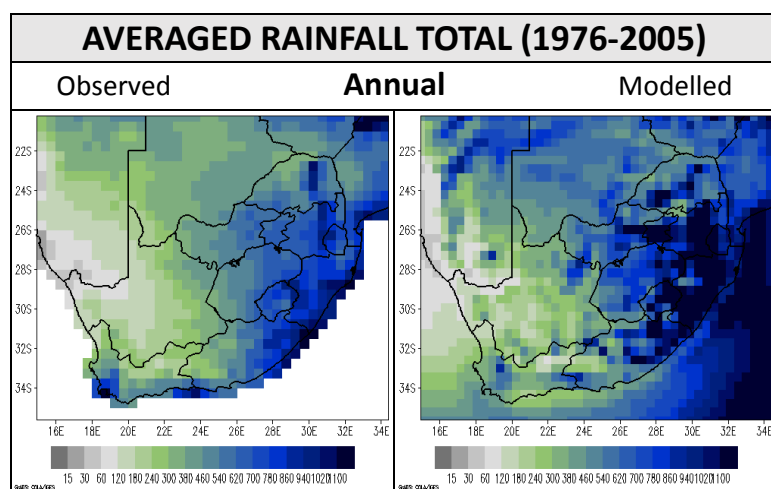
Figure 1: Average of observed annual total rainfall (mm.year^{-1}), from the Global Precipitation Climatology Centre (GPCC) (left), compared to the associated nine-member ensemble mean rainfall as simulated by the RCA4 RCM (right), for the period 1976-2005.
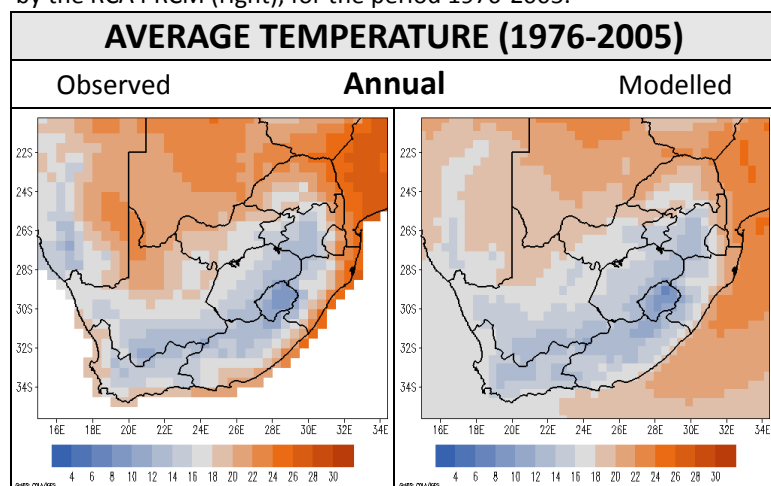
Figure 2: Average of observed annual mean temperature (°C), from the NOAA GHCN_CAMS Land Temperature Analysis (left), compared to the associated nine-member ensemble mean temperature as simulated by the RCA4 RCM (right), for the period 1976-2005.

According to Figure 1, the spatial rainfall distribution of higher rainfall totals in the east, compared to the west, are captured in the model simulations. The simulated rainfall is, however, is slightly overestimated in most part of the country, including for Botswana and Namibia. Values are more realistic in the west, although rainfall is lower than observed in the Cape Town region.

The model performed very well in the simulation of temperatures (Figure 2). The cooler conditions in the Lesotho highlands are captured, as well as he warmer conditions in the northern and north-eastern parts of the country.
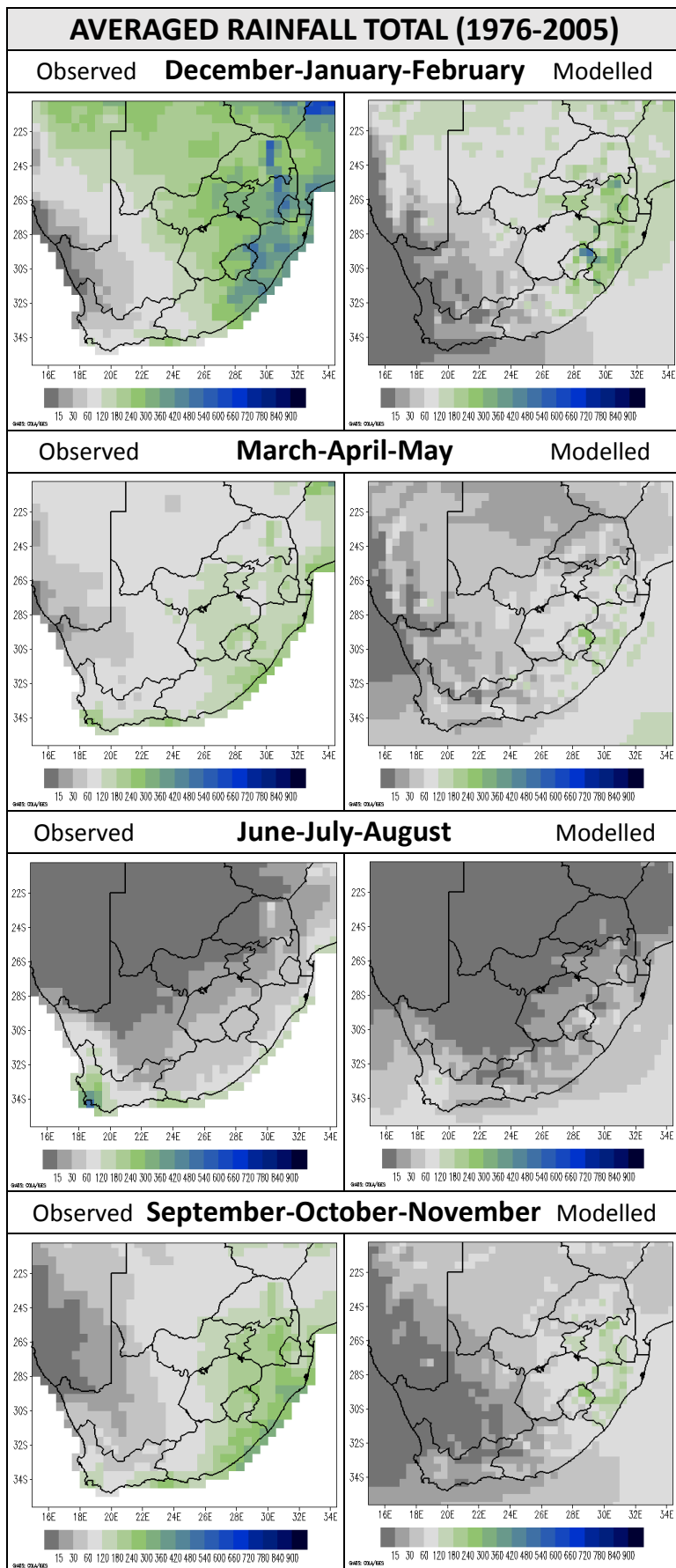
In general, the model succeeded in reproducing the most important annual rainfall and temperature fields, although biases occur in some areas – especially as far as rainfall is concerned.

Figure 3: Average of observed seasonal mean temperature (°C), from the NOAA GHCN_CAMS Land Temperature Analysis (left), compared to the associated nine-member ensemble mean temperature as simulated by the RCA4 RCM (right), for the period 1976-2005.
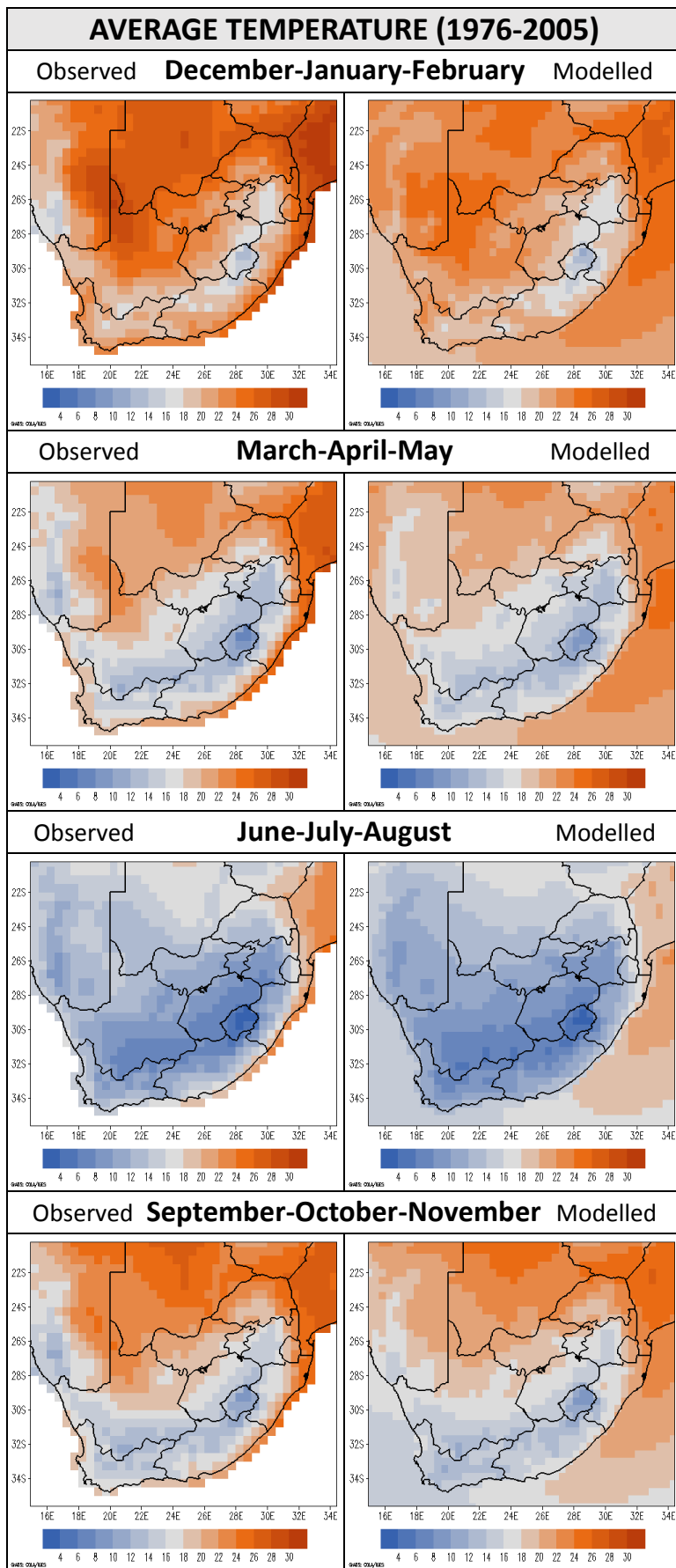
Secondly, seasonal model simulated results were compared with observations (Figures 3 and 4). Both in terms of spatial distribution and magnitude of values, the model, again, performed well in generating realistic temperature fields. In both observations and model simulated maps, the warmest season is indicated as DJF, while the coldest season is indicated as JJA. For DJF, the model succeeded in capturing the hot conditions experienced in the north-western Kalahari region, although slightly lower than observed, while the cooler temperatures in the Lesotho highlands have also been generated in model simulations. The same applies for autumn (MAM), but again with slightly lower temperatures in the Kalahari area in the model field. In general, winter (JJA) temperatures are well-represented since there is a very good agreement between observations and model simulations. Observations and model simulation results for spring (SON) is again highly comparable.

## AVERAGED RAINFALL TOTAL (1976-2005)

Across most of the country, model simulated rainfall for DJF are slightly lower than observed, although the east-west gradient in rainfall is adequately represented. Note the higher rainfall values against the edges of high topography (e.g. north-eastern Lesotho) which occur in both observational and model fields. Autumn (MAM), which is the transition period between summer and winter, denote slightly higher rainfall in the observed east and Western Cape region. Winter (JJA) rainfall is higher in the Cape Town region in the observations, compared to the model simulations. However, the dry conditions in the rest of the country that characterises the winter season are well-captures in the model simulations. For spring (SON) observed rainfall is slightly higher in the observed map, compared to the model simulations. In general, the model succeeded in capturing the major spatial rainfall patterns, as well as the seasonal cycle of a wetter/drier summer in the east/west, and a drier/wetter winter in the east/west.

Figure 4: Average of observed seasonal total rainfall (mm/3-month season), from the Global Precipitation Climatology Centre (GPCC: www.gpcc.dwd.de) (left), compared to the associated nine-member ensemble mean rainfall as simulated by the RCA4 RCM (right), for the period 1976-2005.

PAGE REFERENCE TABLE

Mean temperature change (°C) of the ▪ 90% percentile ▪ Median ▪ 10% percentile	**Period 1: 2036 – 2065**	**RCP 4.5**	**Annual** *(page 11)*	**DJF**	*(page 13)*	**JJA**	*(page 14)*
				MAM	*(page 13)*	**SON**	*(page 14)*
		RCP 8.5	**Annual** *(page 21)*	**DJF**	*(page 23)*	**JJA**	*(page 24)*
				MAM	*(page 23)*	**SON**	*(page 24)*
	Period 2: 2066 – 2095	**RCP 4.5**	**Annual** *(page 11)*	**DJF**	*(page 15)*	**JJA**	*(page 16)*
				MAM	*(page 15)*	**SON**	*(page 16)*
		RCP 8.5	**Annual** *(page 21)*	**DJF**	*(page 25)*	**JJA**	*(page 26)*
				MAM	*(page 25)*	**SON**	*(page 26)*
Total rainfall change (mm) of the ▪ 90% percentile ▪ Median ▪ 10% percentile	**Period 1: 2036 – 2065**	**RCP 4.5**	**Annual** *(page 12)*	**DJF**	*(page 17)*	**JJA**	*(page 18)*
				MAM	*(page 17)*	**SON**	*(page 18)*
		RCP 8.5	**Annual** *(page 22)*	**DJF**	*(page 27)*	**JJA**	*(page 28)*
				MAM	*(page 27)*	**SON**	*(page 28)*
	Period 2: 2066 – 2095	**RCP 4.5**	**Annual** *(page 12)*	**DJF**	*(page 19)*	**JJA**	*(page 20)*
				MAM	*(page 19)*	**SON**	*(page 20)*
		RCP 8.5	**Annual** *(page 22)*	**DJF**	*(page 29)*	**JJA**	*(page 30)*
				MAM	*(page 29)*	**SON**	*(page 30)*
Percentage (%) change in total rainfall	**Period 1: 2036 – 2065**	**RCP 4.5**	**Annual** *(page 31)*	**DJF**	*(page 33)*	**JJA**	*(page 34)*
				MAM	*(page 33)*	**SON**	*(page 34)*
		RCP 8.5	**Annual** *(page 32)*	**DJF**	*(page 35)*	**JJA**	*(page 36)*
				MAM	*(page 35)*	**SON**	*(page 36)*
	Period 2: 2066 – 2095	**RCP 4.5**	**Annual** *(page 31)*	**DJF**	*(page 33)*	**JJA**	*(page 34)*
				MAM	*(page 33)*	**SON**	*(page 34)*
		RCP 8.5	**Annual** *(page 32)*	**DJF**	*(page 35)*	**JJA**	*(page 36)*
				MAM	*(page 35)*	**SON**	*(page 36)*

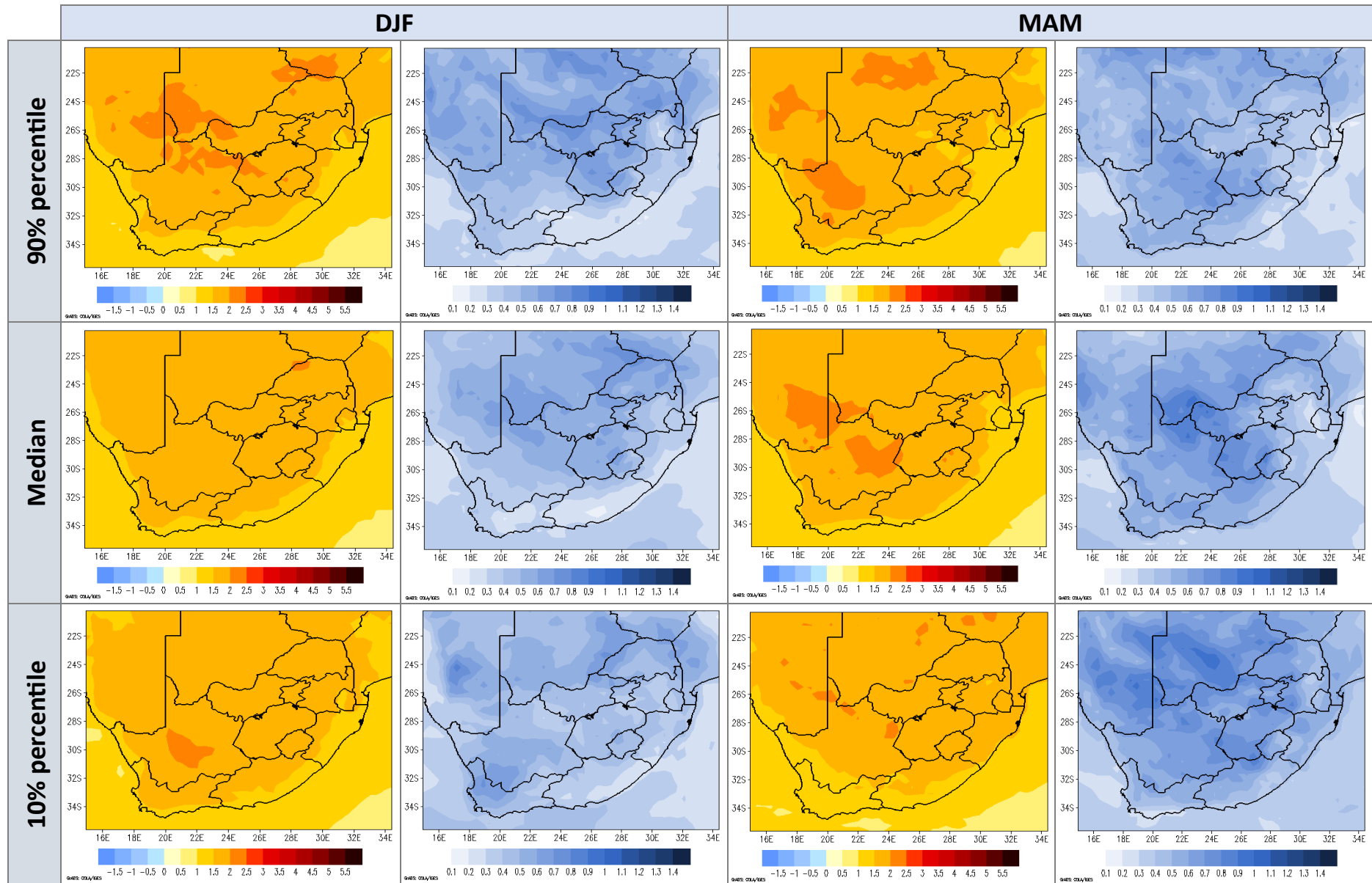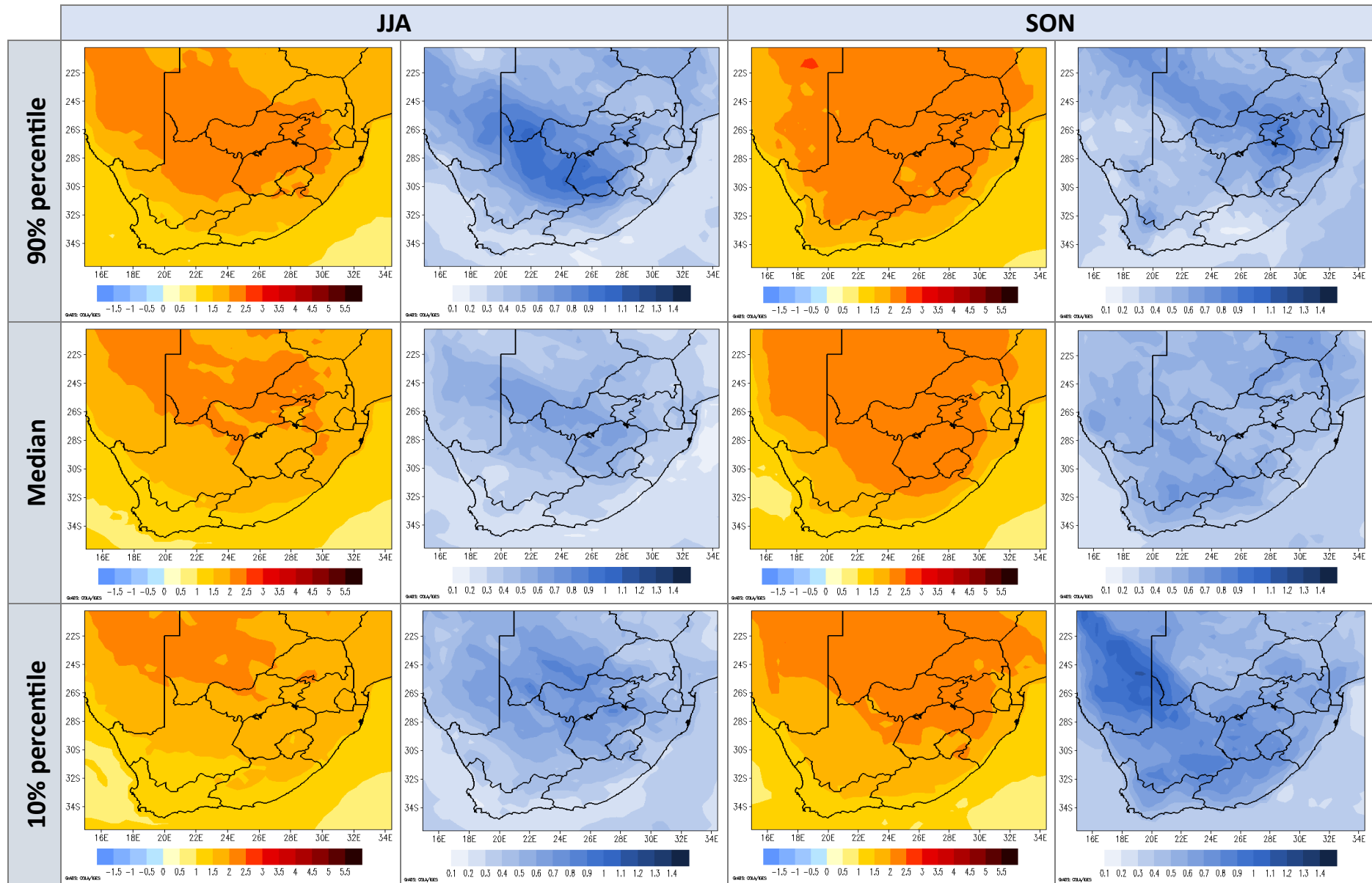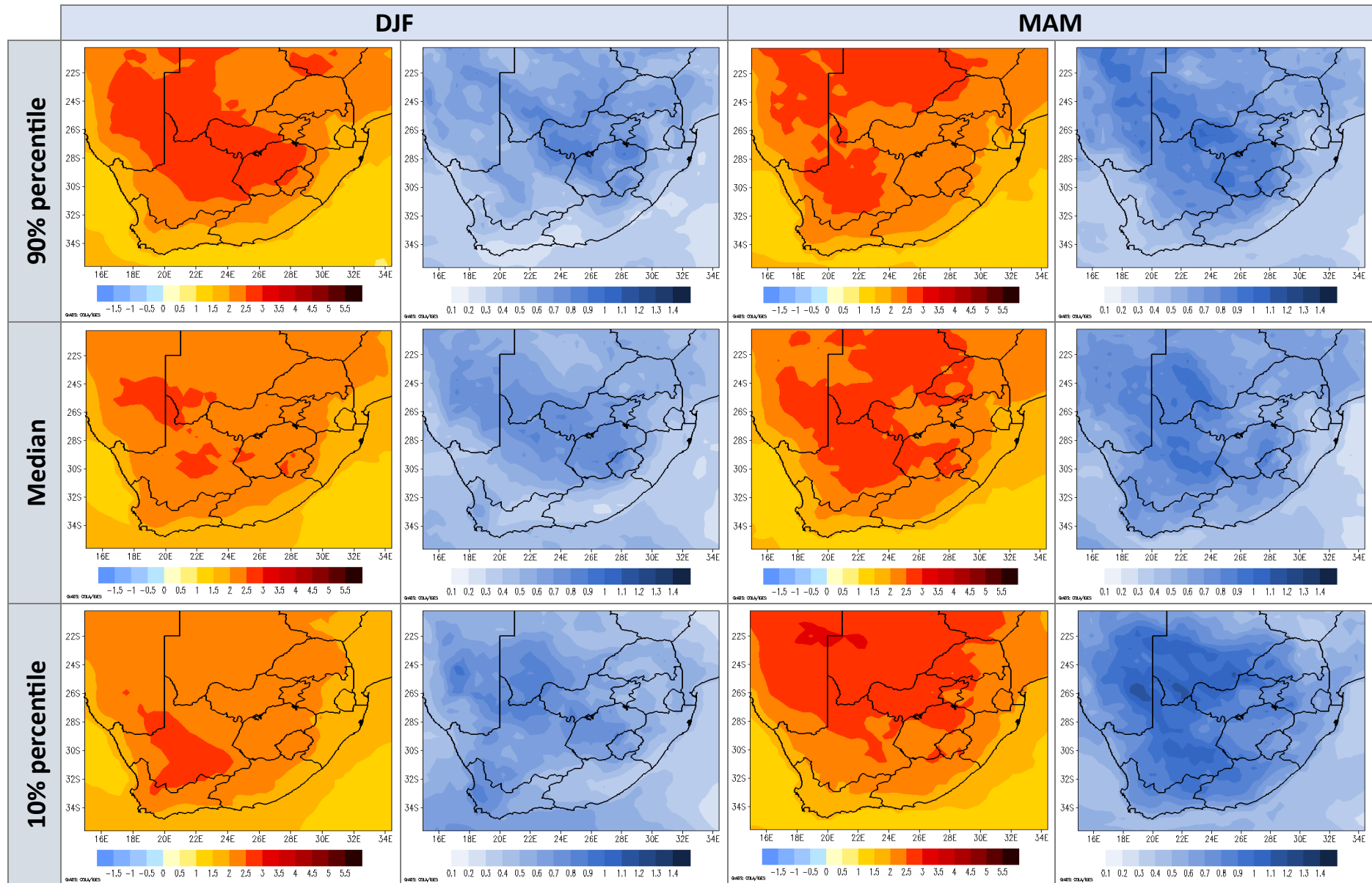**RCP 4.5:** **Annual mean temperature change (ºC)** relative to 1976-2005
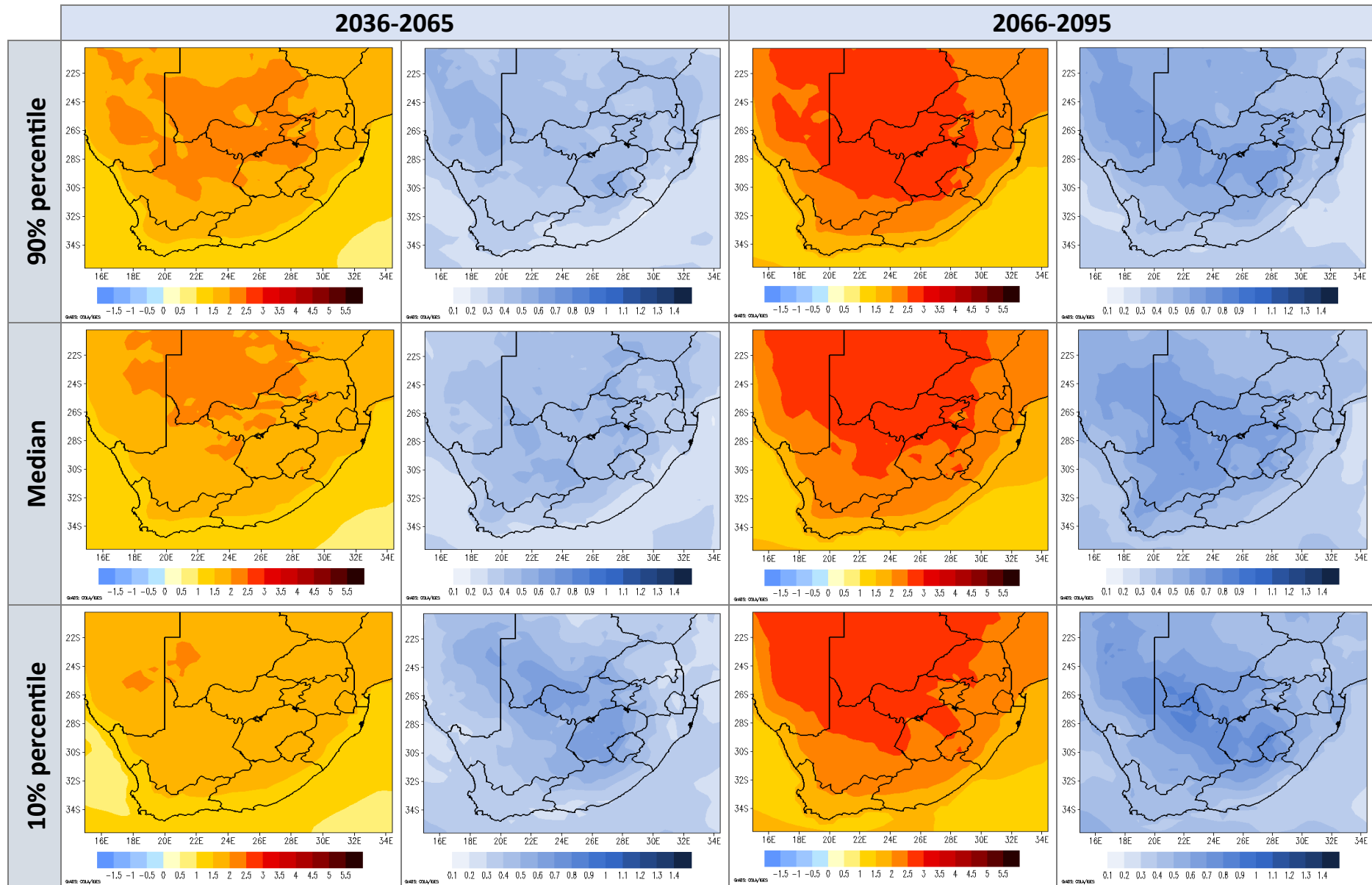
Figure 5: Annual mean near-surface (2m) temperature (°C) change (1st and 3rd columns) from the median (middle row) and the 10% and 90% percentiles (bottom and top rows, respectively) projected for 2036-2065 (left) and 2066-2095 (right), relative to present (1976-2005), under conditions of the RCP 4.5 pathway. The corresponding root-mean-square difference (rmsd) in °C between the nine ensemble member change anomalies is indicated by the maps in the 2nd and 4th columns.

RCP 4.5: **Annual total rainfall change (mm per year)** relative to 1976-2005
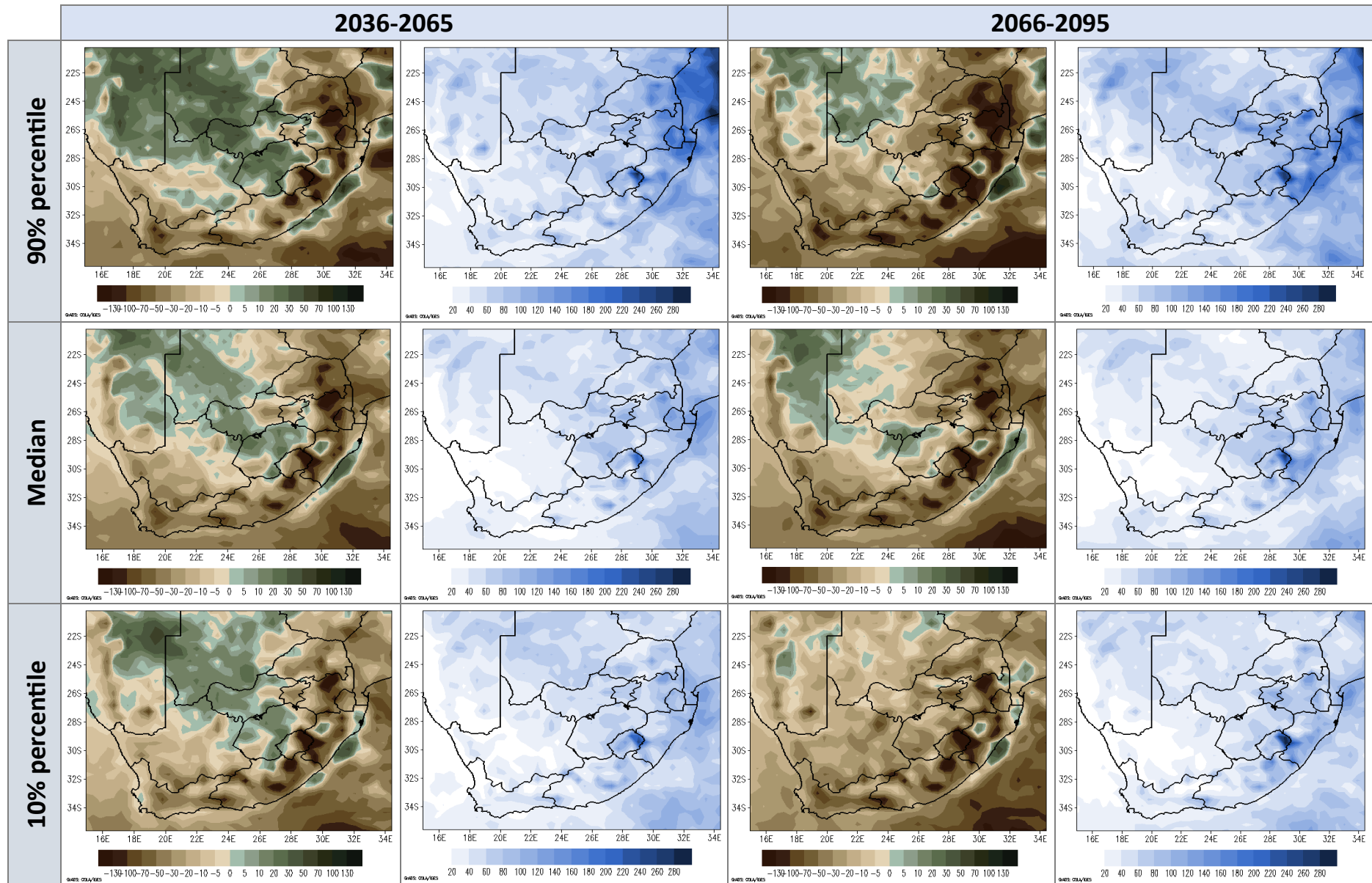
Figure 6: Annual total rainfall (mm per year) change (1st and 3rd columns) from the median (middle row) and the 10% and 90% percentiles (bottom and top rows, respectively) projected for 2036-2065 (left) and 2066-2095 (right), relative to present (1976-2005), under conditions of the RCP 4.5 pathway. The corresponding root-mean-square difference (rmsd) in mm per year between the nine ensemble member change anomalies is indicated by the maps in the 2nd and 4th columns.

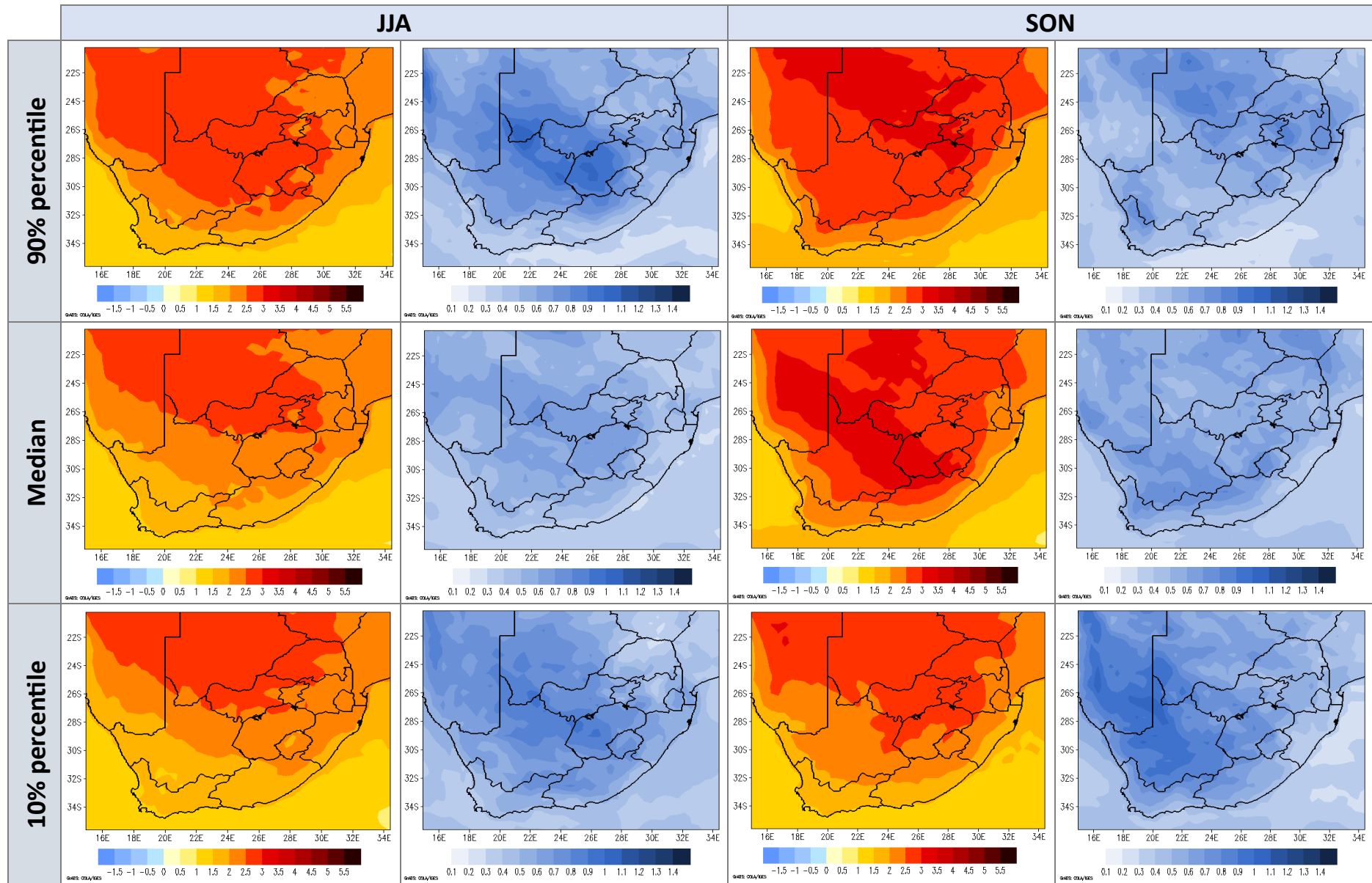**RCP 4.5:** **Seasonal mean temperature change (ºC) for 2036 – 2065** - relative to 1975-2005

Figure 7: Seasonal mean near-surface (2m) temperature (°C) change (1st and 3rd columns) from the median (middle row) and the 10% and 90% percentiles (bottom and top rows, respectively) projected for 2036-2065, relative to present (1976-2005), for the DJF (left) and MAM (right) seasons under conditions of the RCP 4.5 pathway. The corresponding root-mean-square difference (rmsd) in °C between the nine ensemble member change anomalies is indicated by the maps in the 2nd and 4th columns.

13

RCP 4.5: **Seasonal mean temperature change (ºC) for 2036 – 2065** - relative to 1975-2005

Figure 8: Seasonal mean near-surface (2m) temperature (°C) change (1st and 3rd columns) from the median (middle row) and the 10% and 90% percentiles (bottom and top rows, respectively) projected for 2036-2065, relative to present (1976-2005), for the JJA (left) and SON (right) seasons under conditions of the RCP 4.5 pathway. The corresponding root-mean-square difference (rmsd) in °C between the nine ensemble member change anomalies is indicated by the maps in the 2nd and 4th columns.

RCP 4.5: **Seasonal mean temperature change (ºC) for 2066 – 2095** - relative to 1975-2005

Figure 9: Seasonal mean near-surface (2m) temperature (°C) change (1st and 3rd columns) from the median (middle row) and the 10% and 90% percentiles (bottom and top rows, respectively) projected for 2066-2095, relative to present (1976-2005), for the DJF (left) and MAM (right) seasons under conditions of the RCP 4.5 pathway. The corresponding root-mean-square difference (rmsd) in °C between the nine ensemble member change anomalies is indicated by the maps in the 2nd and 4th columns.

RCP 4.5: **Seasonal mean temperature change (ºC) for 2066 – 2095** - relative to 1975-2005

Figure 10: Seasonal mean near-surface (2m) temperature (°C) change (1st and 3rd columns) from the median (middle row) and the 10% and 90% percentiles (bottom and top rows, respectively) projected for 2066-2095, relative to present (1976-2005), for the JJA (left) and SON (right) seasons under conditions of the RCP 4.5 pathway. The corresponding root-mean-square difference (rmsd) in °C between the nine ensemble member change anomalies is indicated by the maps in the 2nd and 4th columns.

RCP 4.5: **Seasonal total rainfall change (mm per season) for 2036 – 2065** - relative to 1975-2005
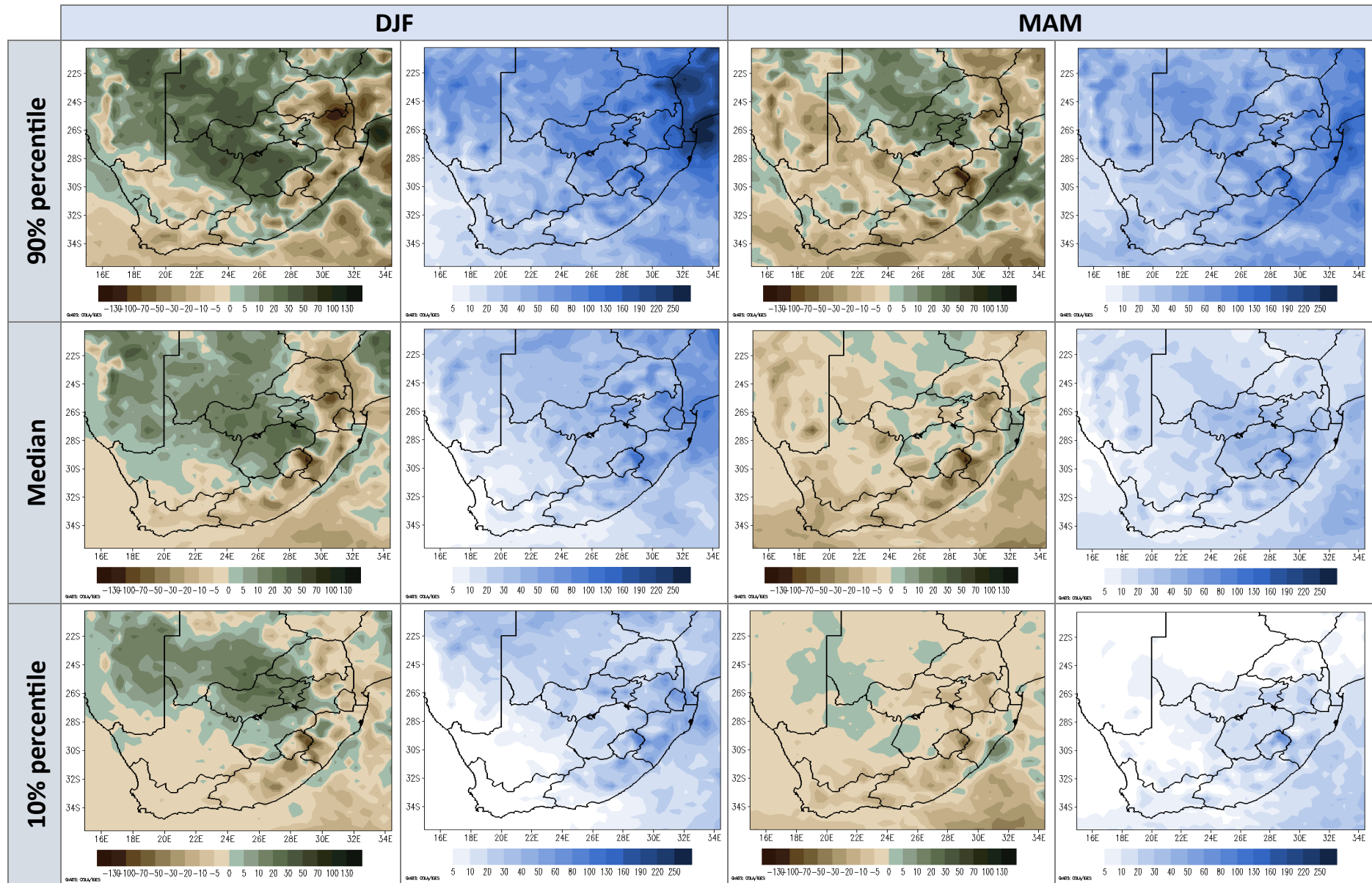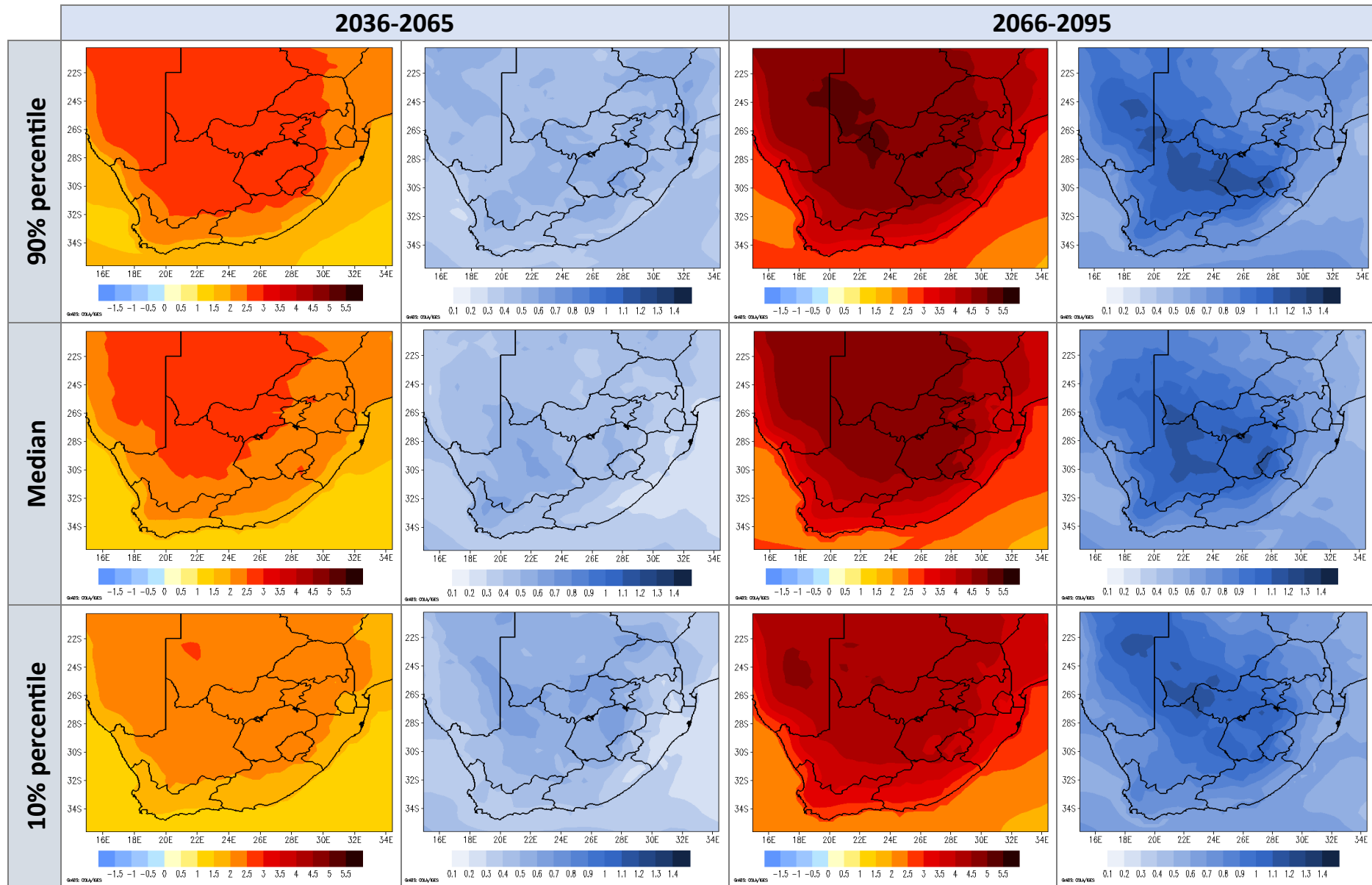

Figure 11: Seasonal total rainfall (mm per 3-month season) change (1st and 3rd columns) from the median (middle row) and the 10% and 90% percentiles (bottom and top rows, respectively) projected for 2036-2065, relative to present (1976-2005), for the DJF (left) and MAM (right) seasons under conditions of the RCP 4.5 pathway. The corresponding root-mean-square difference (rmsd) in °C between the nine ensemble member change anomalies is indicated by the maps in the 2nd and 4th columns.

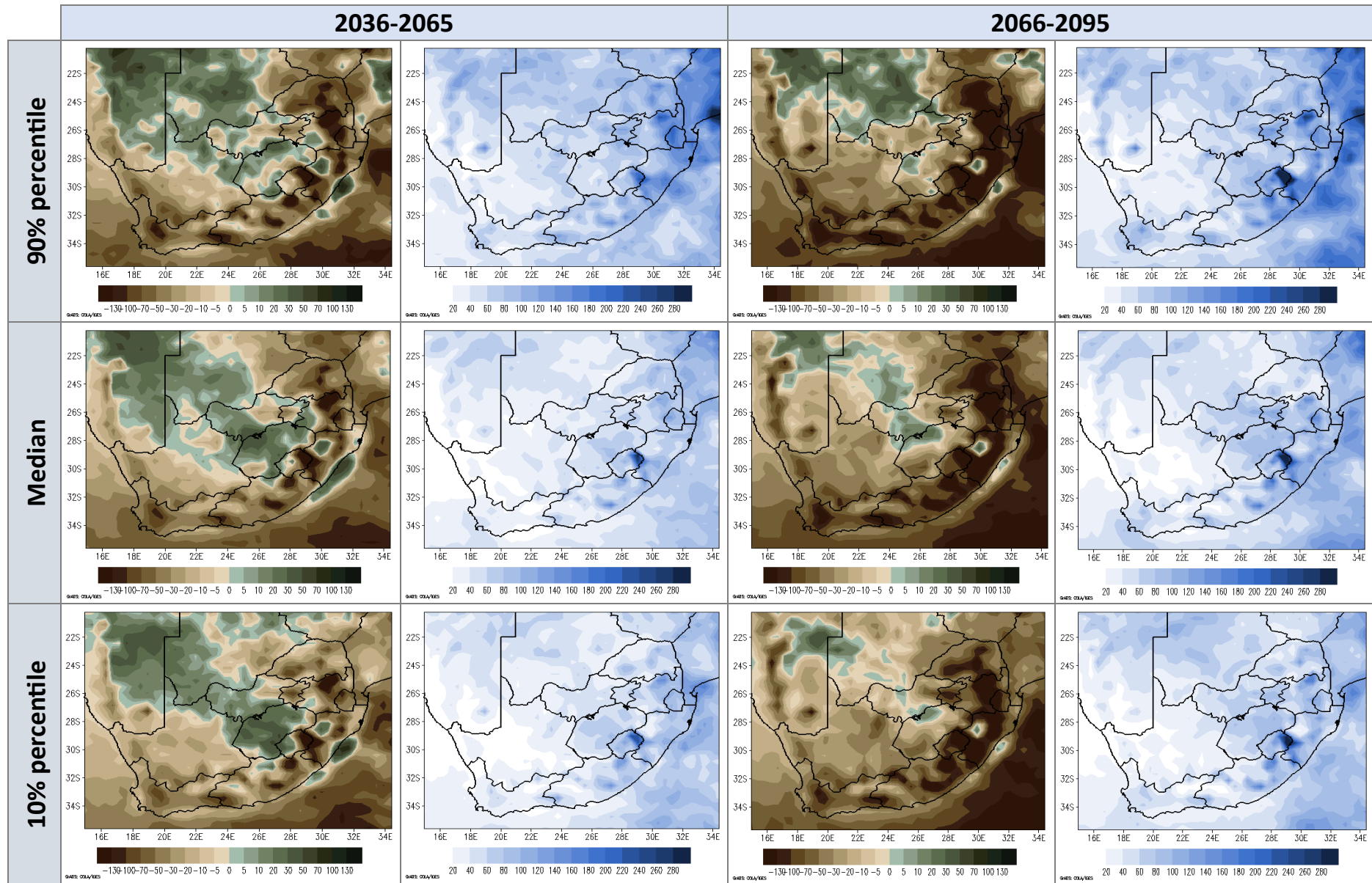**RCP 4.5:** **Seasonal total rainfall change (mm per season) for 2036 – 2065** - relative to 1975-2005
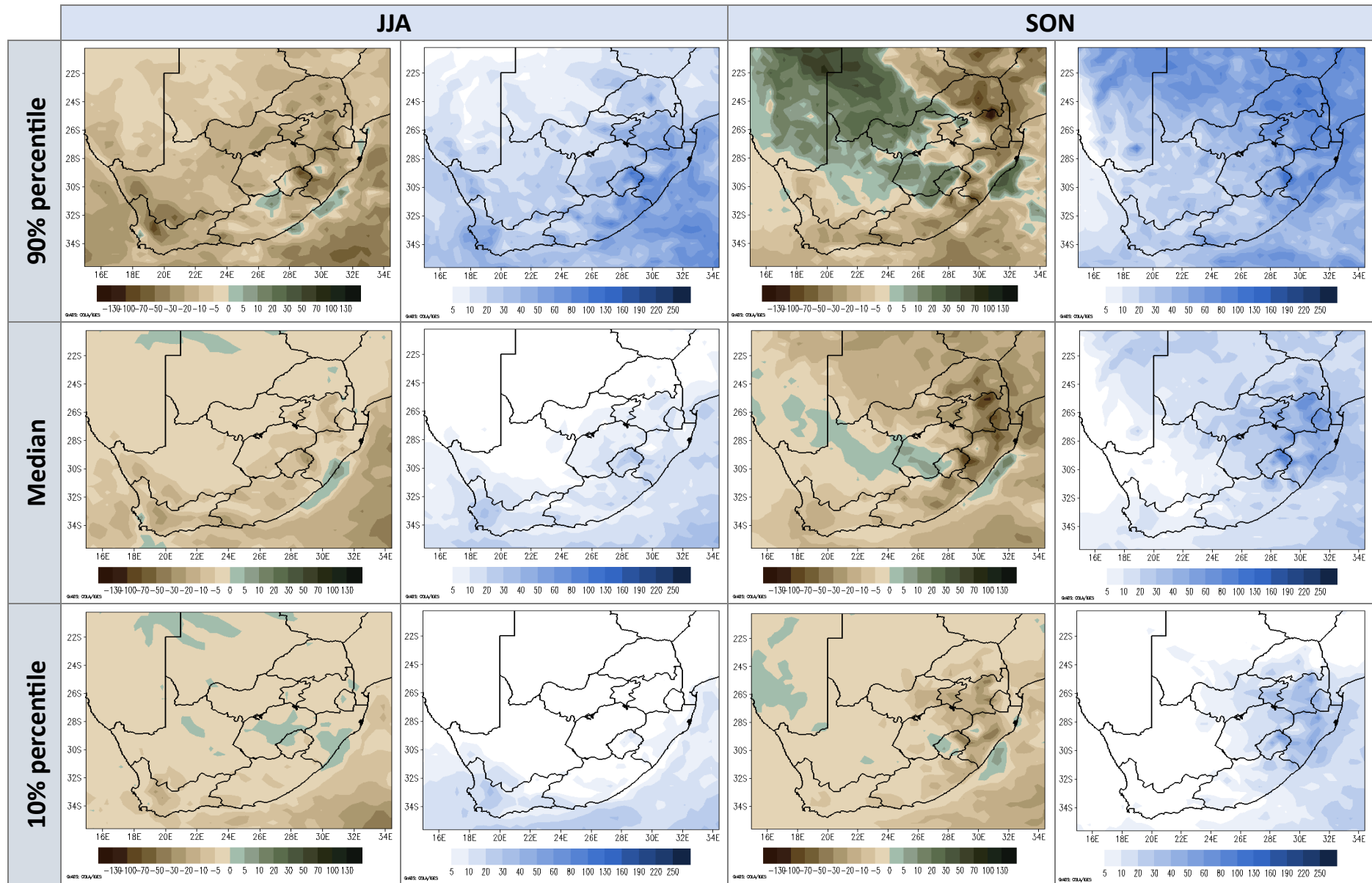
Figure 12: Seasonal total rainfall (mm per 3-month season) change (1st and 3rd columns) from the median (middle row) and the 10% and 90% percentiles (bottom and top rows, respectively) projected for 2036-2065, relative to present (1976-2005), for the JJA (left) and SON (right) seasons under conditions of the RCP 4.5 pathway. The corresponding root-mean-square difference (rmsd) in °C between the nine ensemble member change anomalies is indicated by the maps in the 2nd and 4th columns.

RCP 4.5: **Seasonal total rainfall change (mm per season) for 2066 – 2095** - relative to 1975-2005
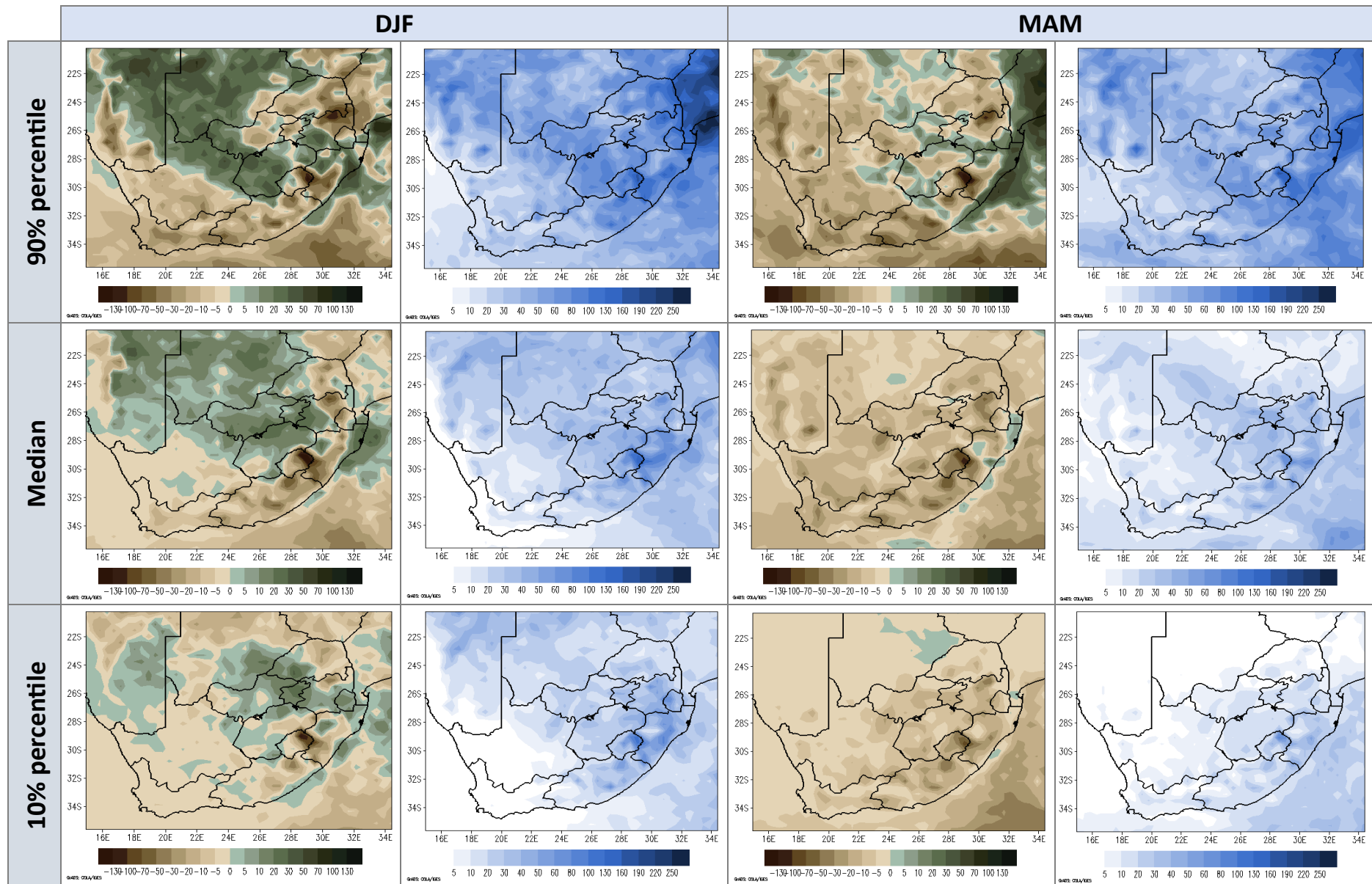
Figure 13: Seasonal total rainfall (mm per 3-month season) change (1st and 3rd columns) from the median (middle row) and the 10% and 90% percentiles (bottom and top rows, respectively) projected for 2066-2095, relative to present (1976-2005), for the DJF (left) and MAM (right) seasons under conditions of the RCP 4.5 pathway. The corresponding root-mean-square difference (rmsd) in °C between the nine ensemble member change anomalies is indicated by the maps in the 2nd and 4th columns.

RCP 4.5: Seasonal total rainfall change (mm per season) for 2066 – 2095 - relative to 1975-2005
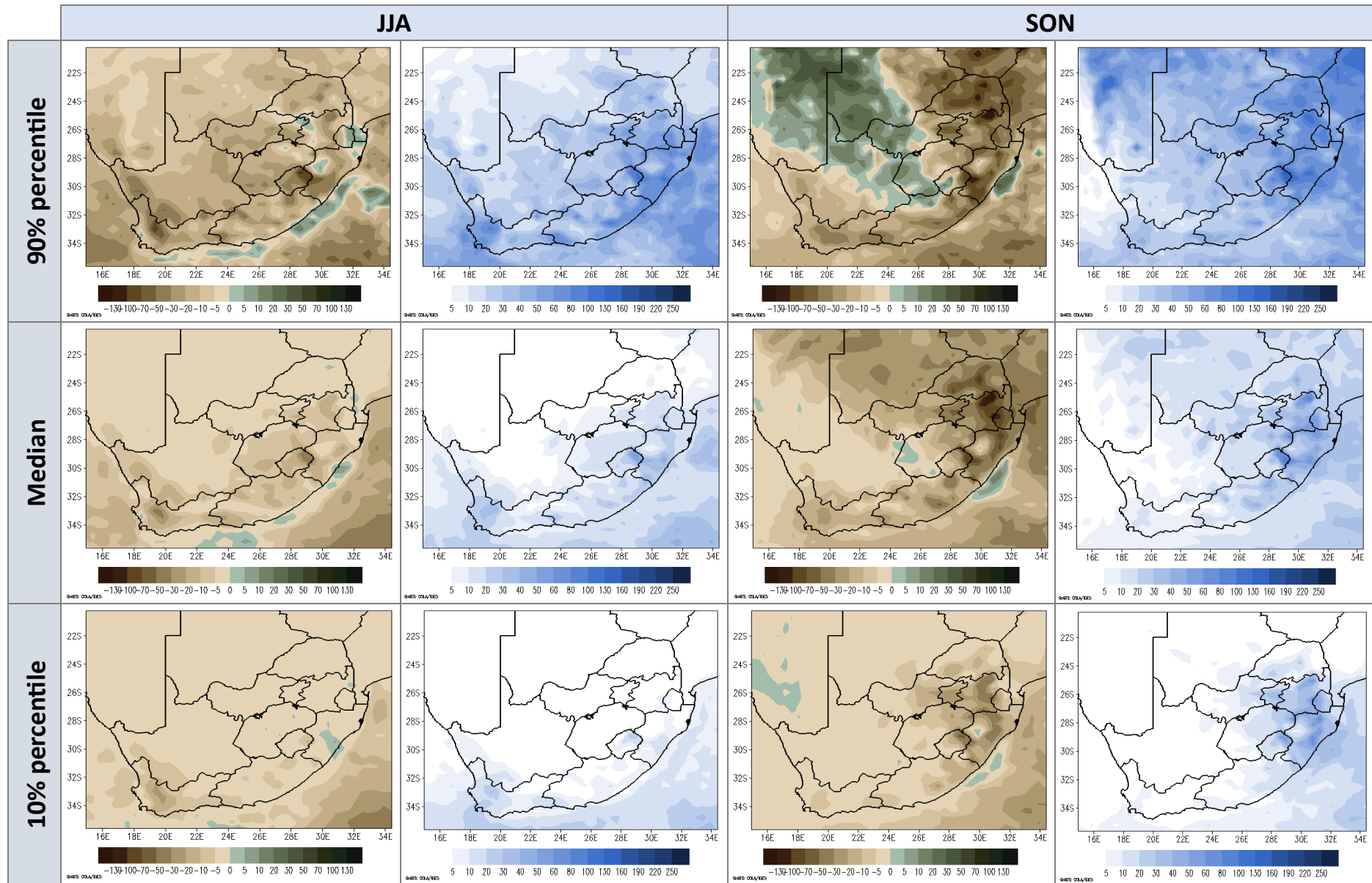
Figure 14: Seasonal total rainfall (mm per 3-month season) change (1st and 3rd columns) from the median (middle row) and the 10% and 90% percentiles (bottom and top rows, respectively) projected for 2066-2095, relative to present (1976-2005), for the JJA (left) and SON (right) seasons under conditions of the RCP 4.5 pathway. The corresponding root-mean-square difference (rmsd) in °C between the nine ensemble member change anomalies is indicated by the maps in the 2nd and 4th columns.

RCP 8.5: **Annual mean temperature change (ºC)** relative to 1976-2005

Figure 15: Annual mean near-surface (2m) temperature (°C) change (1st and 3rd columns) from the median (middle row) and the 10% and 90% percentiles (bottom and top rows, respectively) projected for 2036-2065 (left) and 2066-2095 (right), relative to present (1976-2005), under conditions of the RCP 8.5 pathway. The corresponding root-mean-square difference (rmsd) in °C between the nine ensemble member change anomalies is indicated by the maps in the 2nd and 4th columns.

RCP 8.5: **Annual total rainfall change (mm per year)** relative to 1976-2005

Figure 16: Annual total rainfall (mm per year) change (1st and 3rd columns) from the median (middle row) and the 10% and 90% percentiles (bottom and top rows, respectively) projected for 2036-2065 (left) and 2066-2095 (right), relative to present (1976-2005), under conditions of the RCP 8.5 pathway. The corresponding root-mean-square difference (rmsd) in mm per year between the nine ensemble member change anomalies is indicated by the maps in the 2nd and 4th columns.

RCP 8.5: Seasonal mean temperature change (ºC) for 2036 – 2065 - relative to 1975-2005
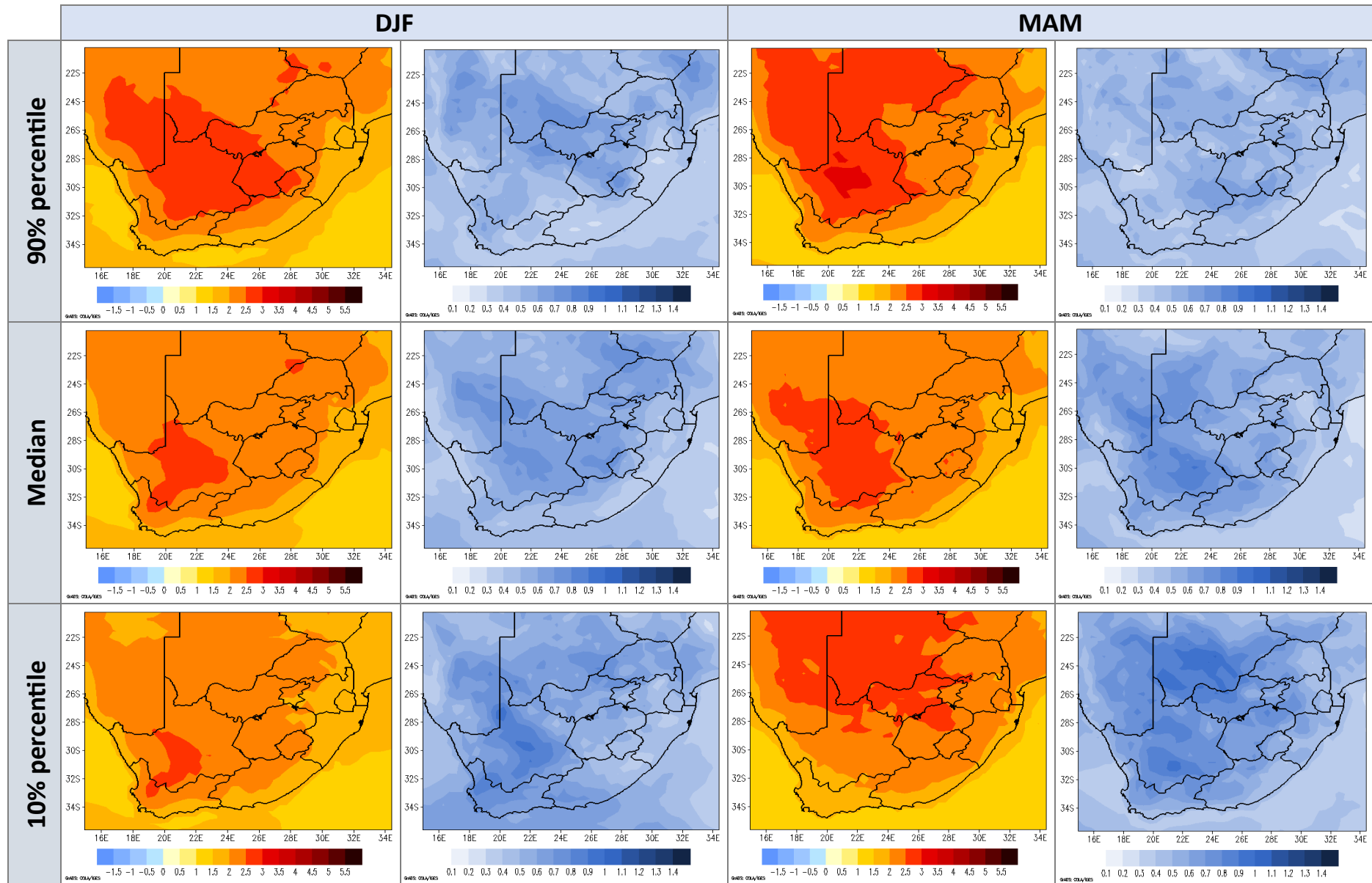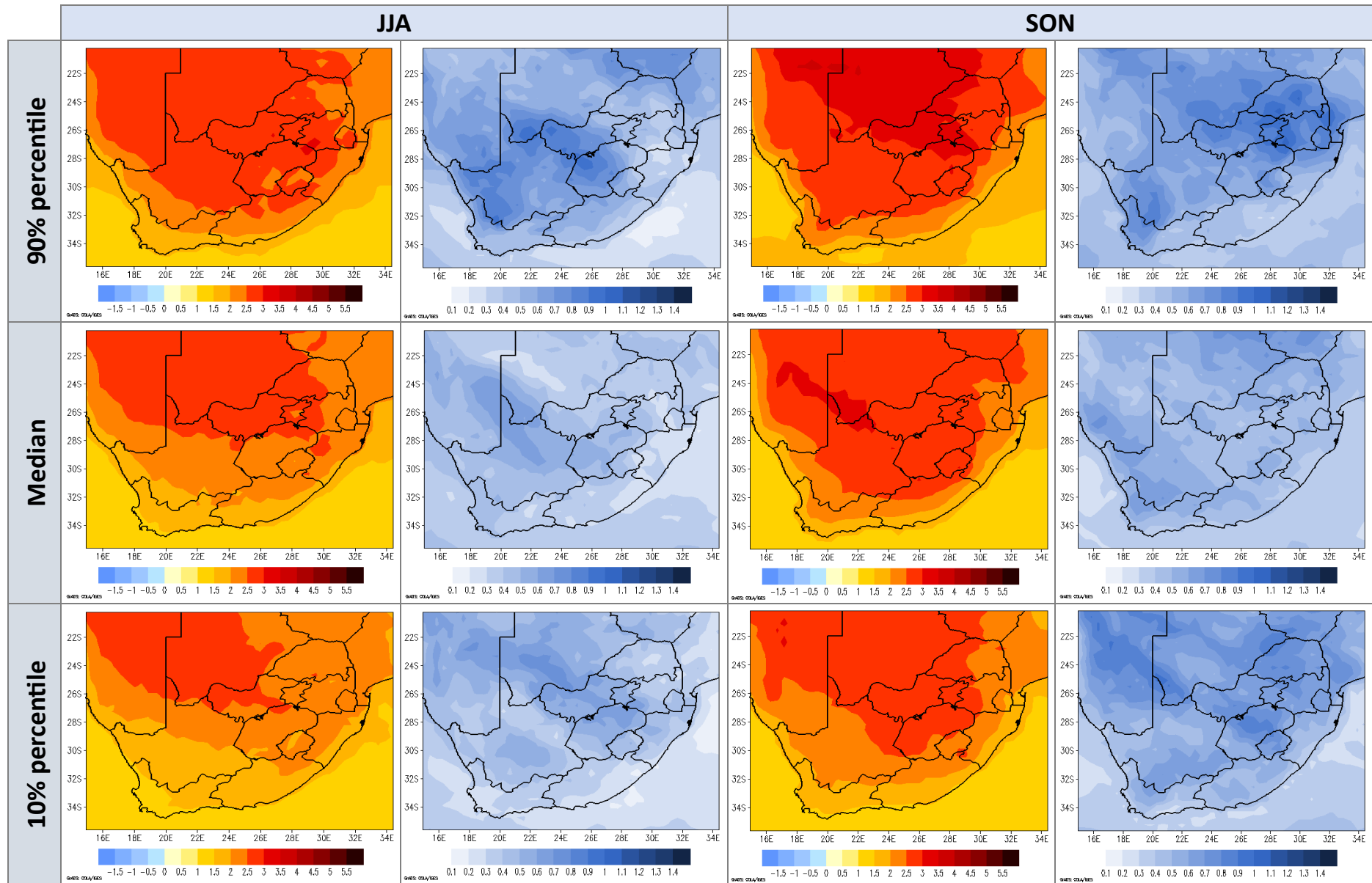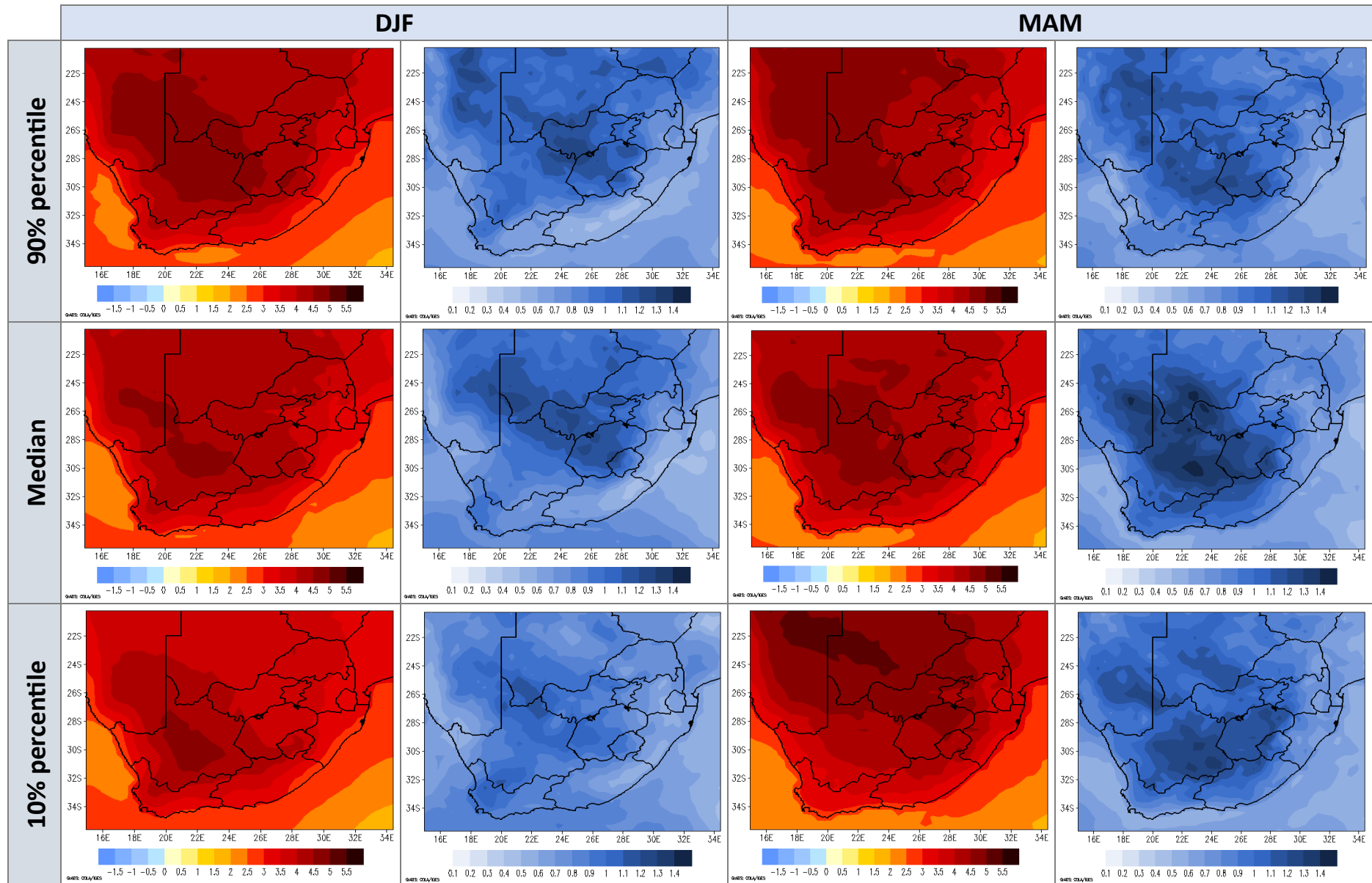

Figure 17: Seasonal mean near-surface (2m) temperature (°C) change (1st and 3rd columns) from the median (middle row) and the 10% and 90% percentiles (bottom and top rows, respectively) projected for 2036-2065, relative to present (1976-2005), for the DJF (left) and MAM (right) seasons under conditions of the RCP 8.5 pathway. The corresponding root-mean-square difference (rmsd) in °C between the nine ensemble member change anomalies is indicated by the maps in the 2nd and 4th columns.
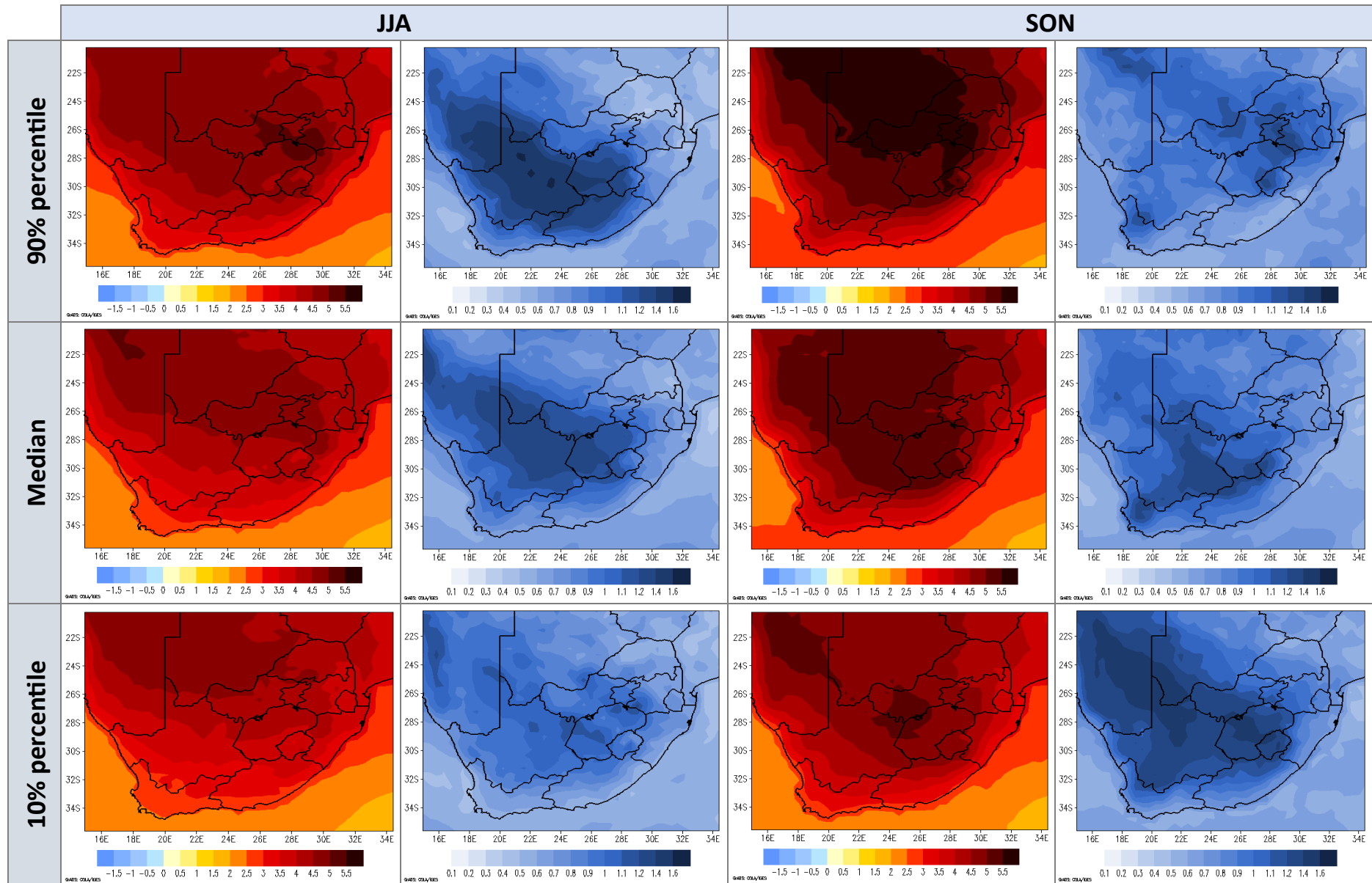
**RCP 8.5:** **Seasonal mean temperature change (ºC) for 2036 – 2065** - relative to 1975-2005

Figure 18: Seasonal mean near-surface (2m) temperature (°C) change (1st and 3rd columns) from the median (middle row) and the 10% and 90% percentiles (bottom and top rows, respectively) projected for 2036-2065, relative to present (1976-2005), for the JJA (left) and SON (right) seasons under conditions of the RCP 8.5 pathway. The corresponding root-mean-square difference (rmsd) in °C between the nine ensemble member change anomalies is indicated by the maps in the 2nd and 4th columns.

**RCP 8.5:** **Seasonal mean temperature change (ºC) for 2066 – 2095** - relative to 1975-2005

Figure 19: Seasonal mean near-surface (2m) temperature (°C) change (1st and 3rd columns) from the median (middle row) and the 10% and 90% percentiles (bottom and top rows, respectively) projected for 2066-2095, relative to present (1976-2005), for the DJF (left) and MAM (right) seasons under conditions of the RCP 8.5 pathway. The corresponding root-mean-square difference (rmsd) in °C between the nine ensemble member change anomalies is indicated by the maps in the 2nd and 4th columns.

RCP 8.5: **Seasonal mean temperature change (ºC) for 2066 – 2095** - relative to 1975-2005

Figure 20: Seasonal mean near-surface (2m) temperature (°C) change (1st and 3rd columns) from the median (middle row) and the 10% and 90% percentiles (bottom and top rows, respectively) projected for 2066-2095, relative to present (1976-2005), for the JJA (left) and SON (right) seasons under conditions of the RCP 8.5 pathway. The corresponding root-mean-square difference (rmsd) in °C between the nine ensemble member change anomalies is indicated by the maps in the 2nd and 4th columns.

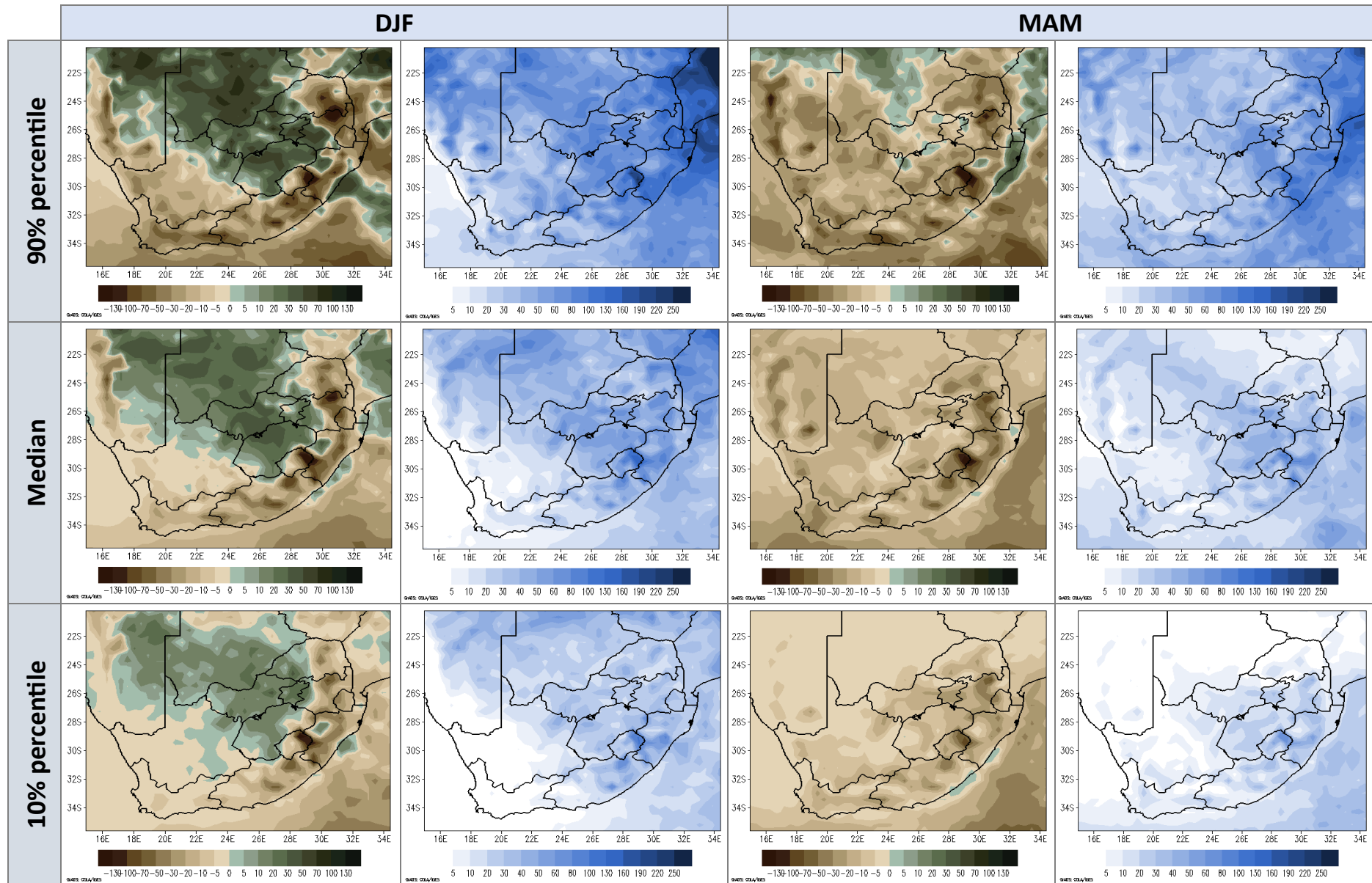**RCP 8.5:** **Seasonal total rainfall change (mm per season) for 2036 – 2065** - relative to 1975-2005
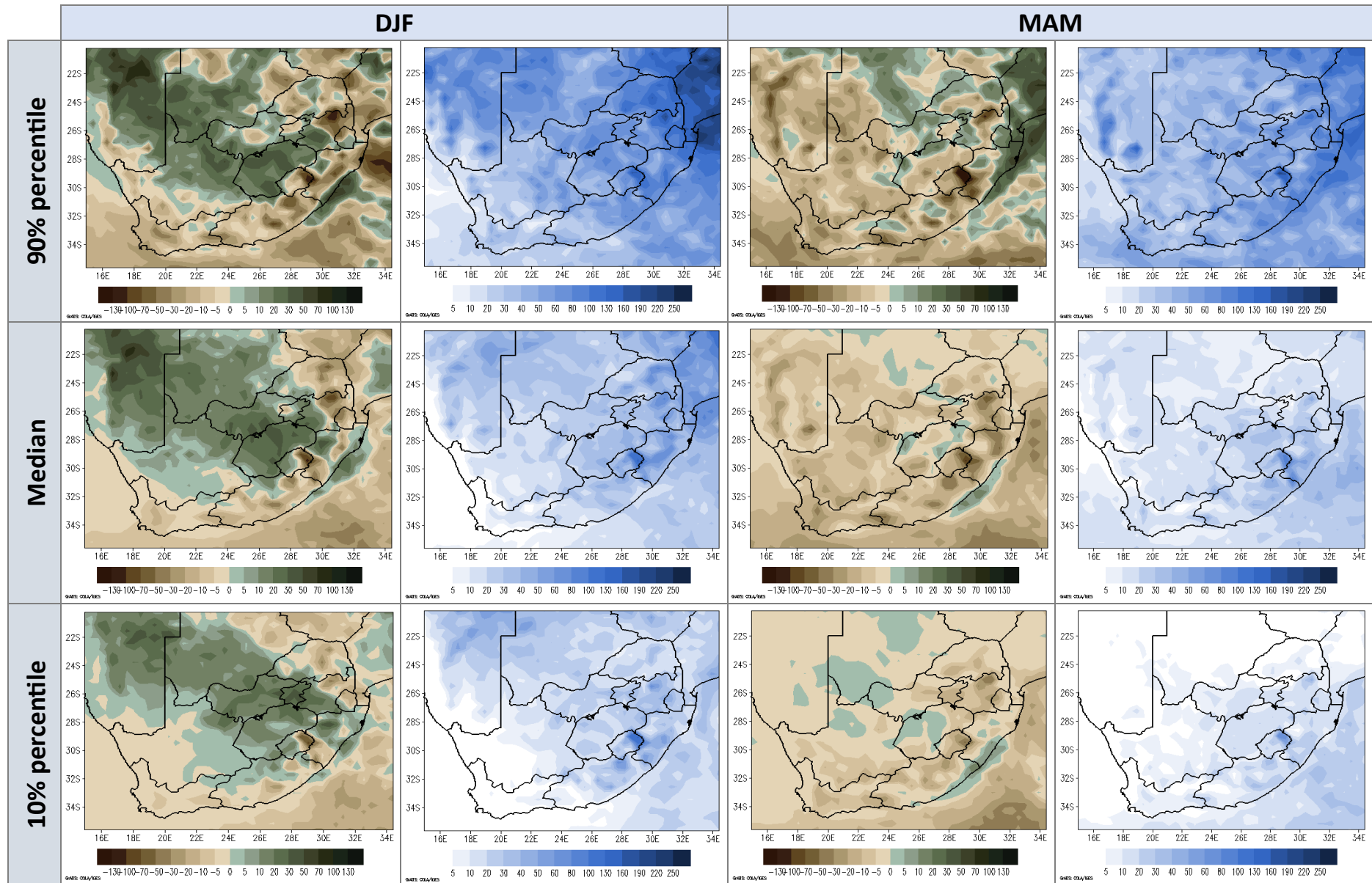
Figure 21: Seasonal total rainfall (mm per 3-month season) change (1st and 3rd columns) from the median (middle row) and the 10% and 90% percentiles (bottom and top rows, respectively) projected for 2036-2065, relative to present (1976-2005), for the DJF (left) and MAM (right) seasons under conditions of the RCP 8.5 pathway. The corresponding root-mean-square difference (rmsd) in °C between the nine ensemble member change anomalies is indicated by the maps in the 2nd and 4th columns.

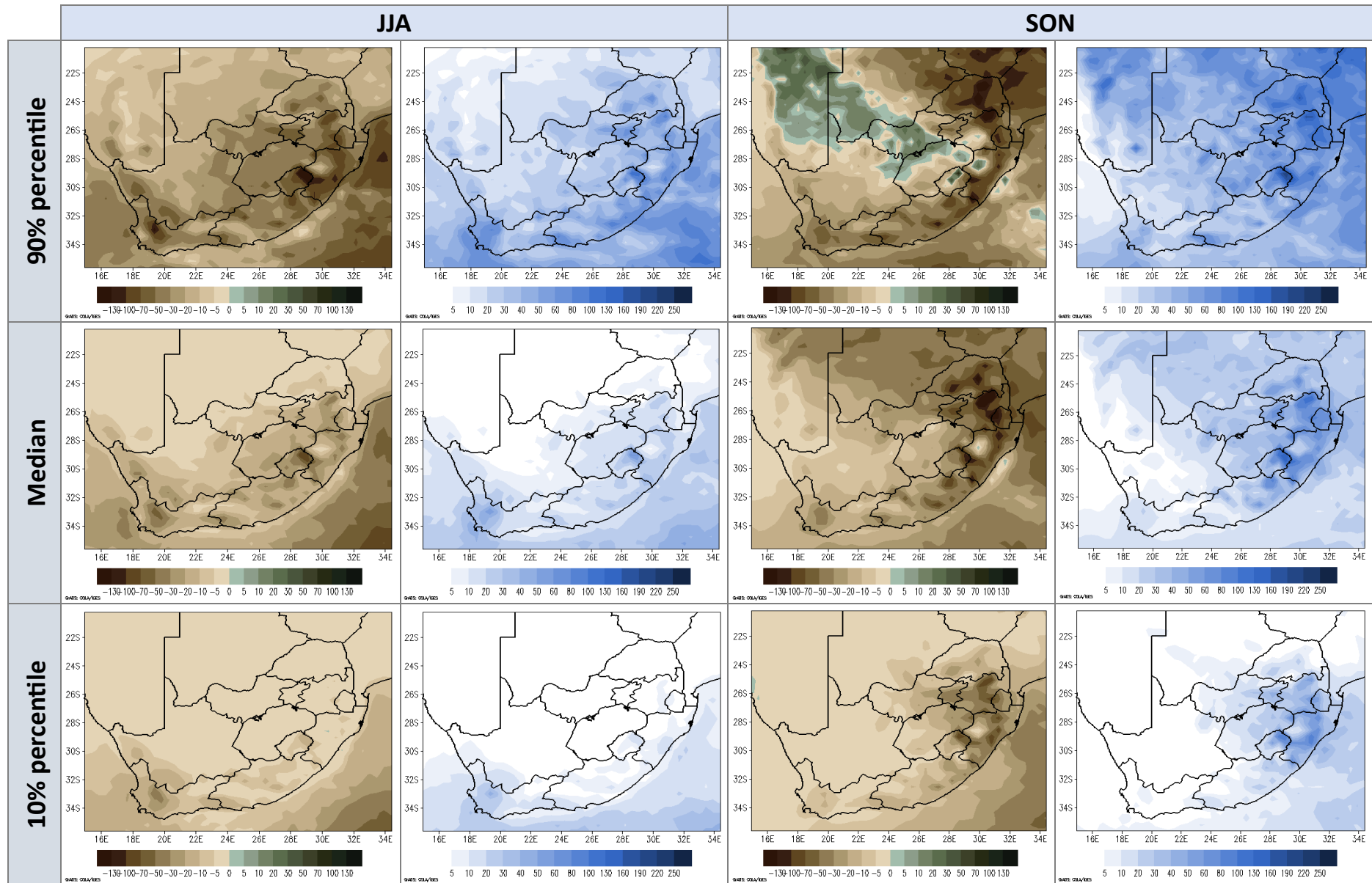**RCP 8.5:** **Seasonal total rainfall change (mm per season) for 2036 – 2065** - relative to 1975-2005
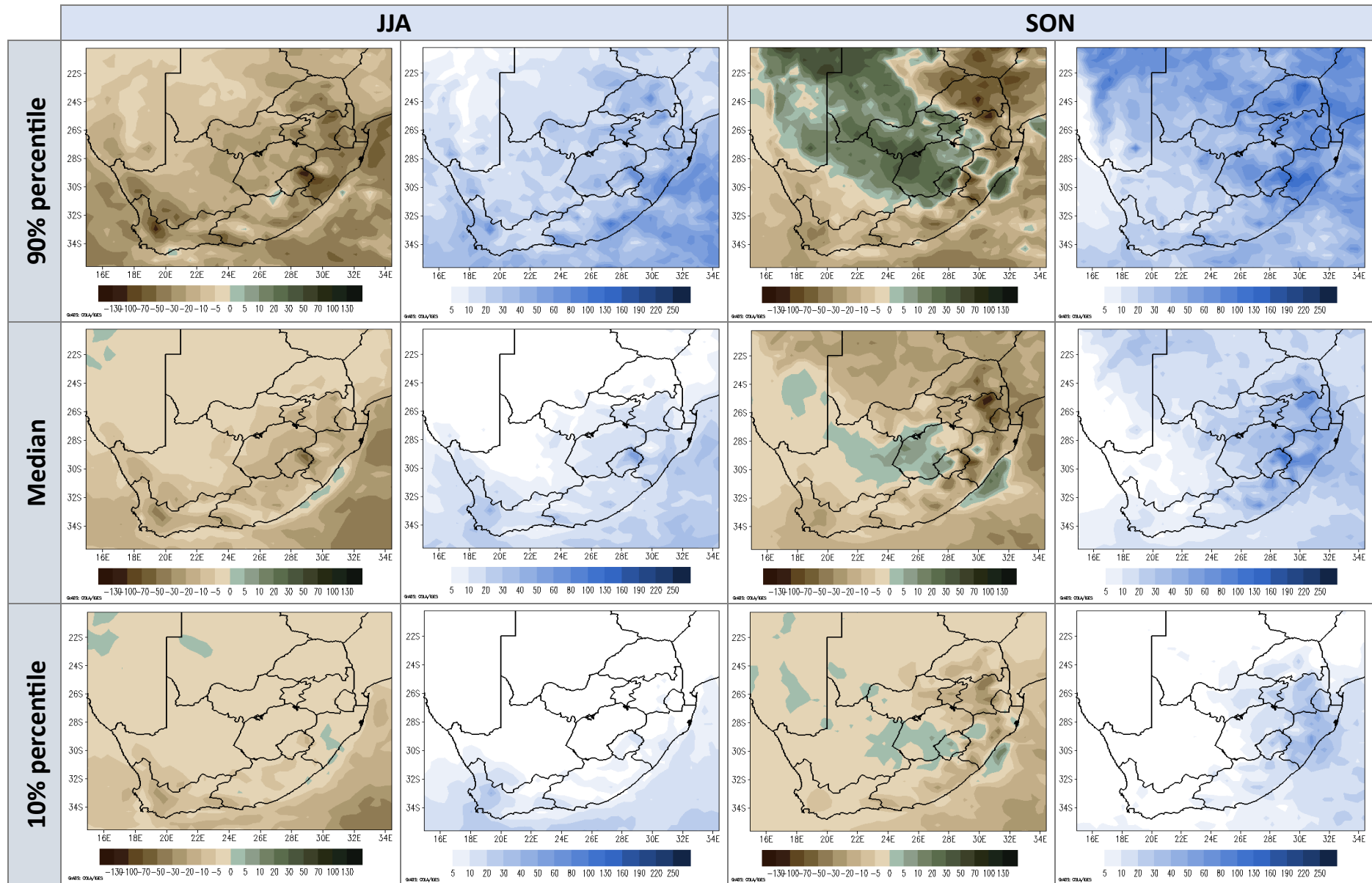
Figure 22: Seasonal total rainfall (mm per 3-month season) change (1st and 3rd columns) from the median (middle row) and the 10% and 90% percentiles (bottom and top rows, respectively) projected for 2036-2065, relative to present (1976-2005), for the JJA (left) and SON (right) seasons under conditions of the RCP 8.5 pathway. The corresponding root-mean-square difference (rmsd) in °C between the nine ensemble member change anomalies is indicated by the maps in the 2nd and 4th columns.

**RCP 8.5:** **Seasonal total rainfall change (mm per season) for 2066 – 2095** - relative to 1975-2005

Figure 23: Seasonal total rainfall (mm per 3-month season) change (1st and 3rd columns) from the median (middle row) and the 10% and 90% percentiles (bottom and top rows, respectively) projected for 2066-2095, relative to present (1976-2005), for the DJF (left) and MAM (right) seasons under conditions of the RCP 8.5 pathway. The corresponding root-mean-square difference (rmsd) in °C between the nine ensemble member change anomalies is indicated by the maps in the 2nd and 4th columns.

**RCP 8.5:** **Seasonal total rainfall change (mm per season) for 2066 – 2095** - relative to 1975-2005

Figure 24: Seasonal total rainfall (mm per 3-month season) change (1st and 3rd columns) from the median (middle row) and the 10% and 90% percentiles (bottom and top rows, respectively) projected for 2066-2095, relative to present (1976-2005), for the JJA (left) and SON (right) seasons under conditions of the RCP 8.5 pathway. The corresponding root-mean-square difference (rmsd) in °C between the nine ensemble member change anomalies is indicated by the maps in the 2nd and 4th columns.

Annual percentage (%) change in total rainfall - relative to 1975-2005
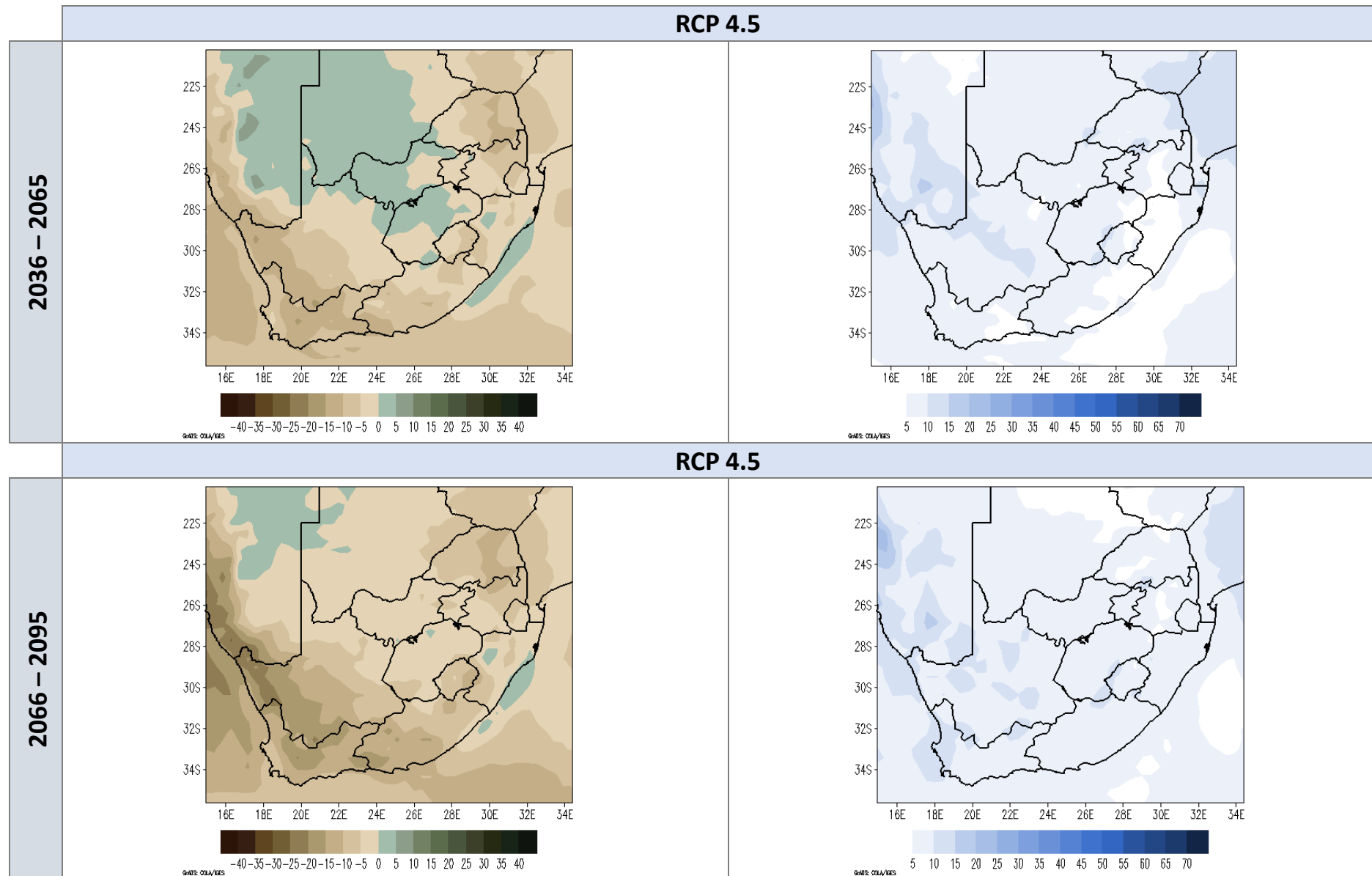
Figure 25: Annual total rainfall percentage (%) change (left) from the median projected for 2036-2065 (top) and 2066-2095 (bottom), relative to present (1976-2005), under conditions of the RCP 4.5 pathway. The corresponding root-mean-square difference (rmsd) in percentage (%) between the nine ensemble member change anomalies is indicated at the right.

31

Annual percentage (%) change in total rainfall - relative to 1975-2005
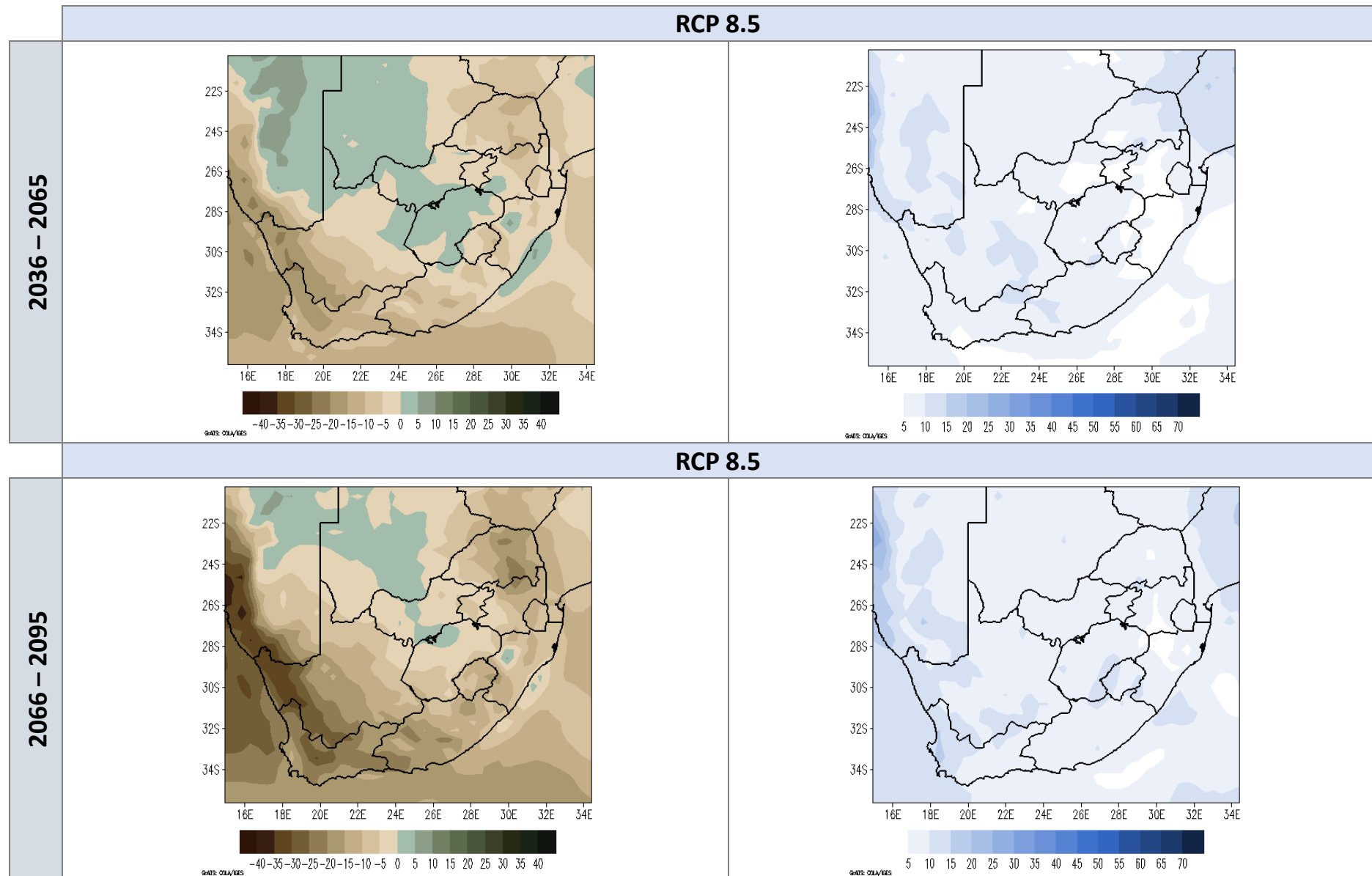
Figure 26: Annual total rainfall percentage (%) change (left) from the median projected for 2036-2065 (top) and 2066-2095 (bottom), relative to present (1976-2005), under conditions of the RCP 8.5 pathway. The corresponding root-mean-square difference (rmsd) in percentage (%) between the nine ensemble member change anomalies is indicated at the right.

RCP 4.5: Seasonal percentage (%) change in total rainfall - relative to 1975-2005
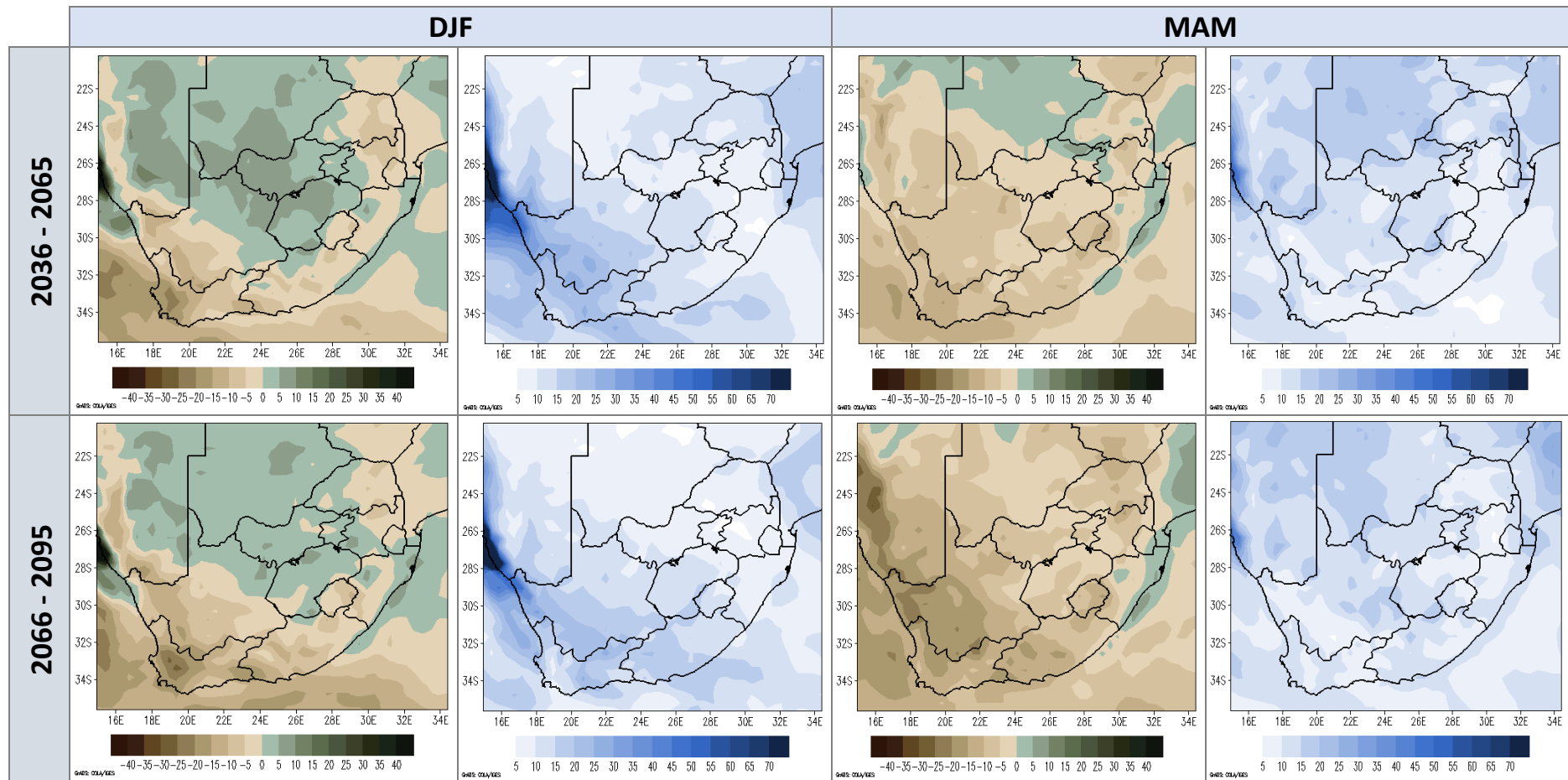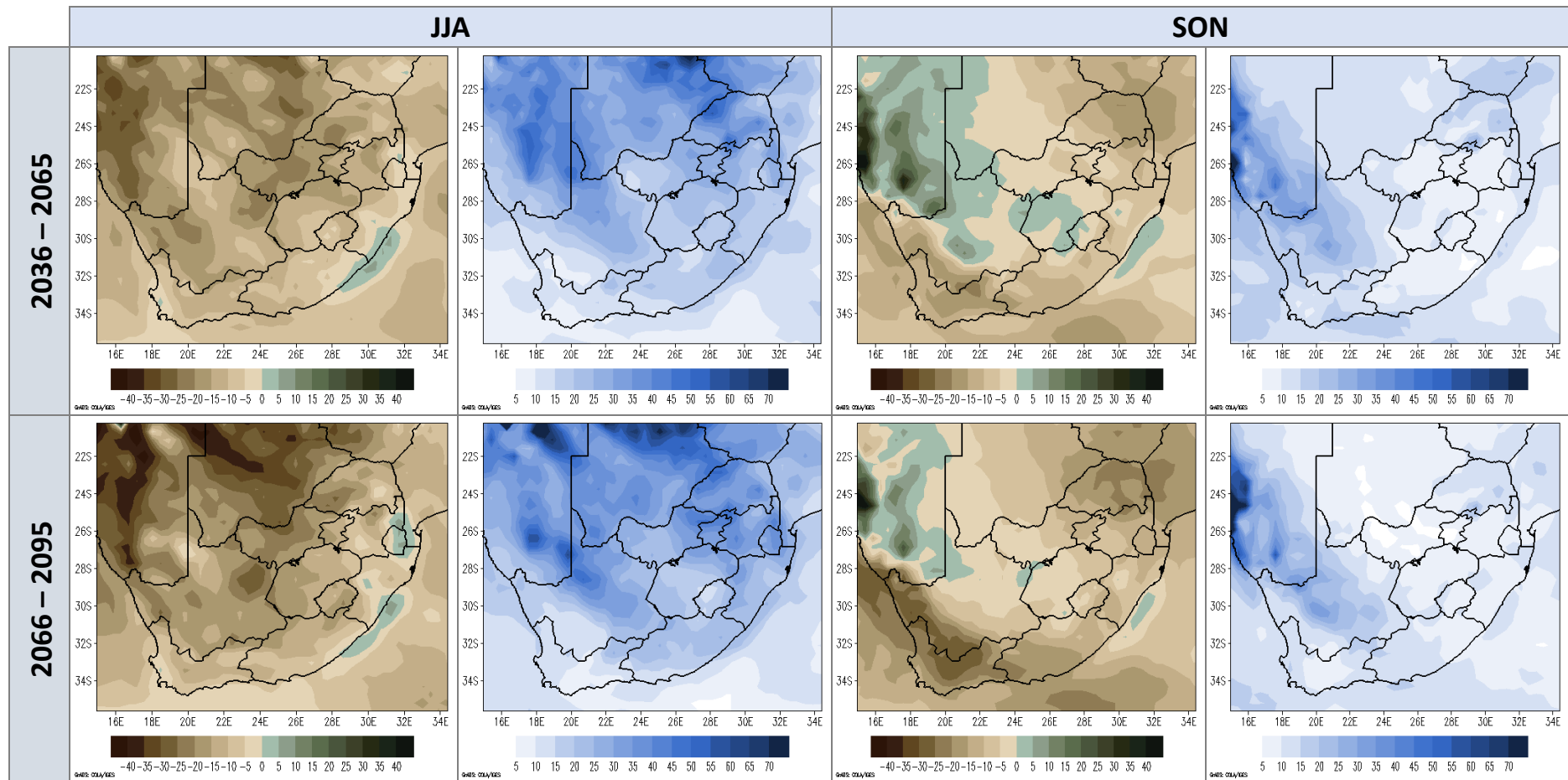

Figure 27: Seasonal total rainfall percentage (%) change (1st and 3rd columns) for the seasons DJF (left) and MAM (right) from the median projected for 2036-2065 (top) and 2066-2095 (bottom), relative to present (1976-2005), under conditions of the RCP 4.5 pathway. The corresponding root-mean-square difference (rmsd) in percentage (%) between the nine ensemble member change anomalies is indicated in the 2nd and 4th columns.

RCP 4.5: Seasonal percentage (%) change in total rainfall - relative to 1975-2005

Figure 28: Seasonal total rainfall percentage (%) change (1st and 3rd columns) for the seasons JJA (left) and SON (right) from the median projected for 2036-2065 (top) and 2066-2095 (bottom), relative to present (1976-2005), under conditions of the RCP 4.5 pathway. The corresponding root-mean-square difference (rmsd) in percentage (%) between the nine ensemble member change anomalies is indicated in the 2nd and 4th columns.

RCP 8.5: Seasonal percentage (%) change in total rainfall - relative to 1975-2005
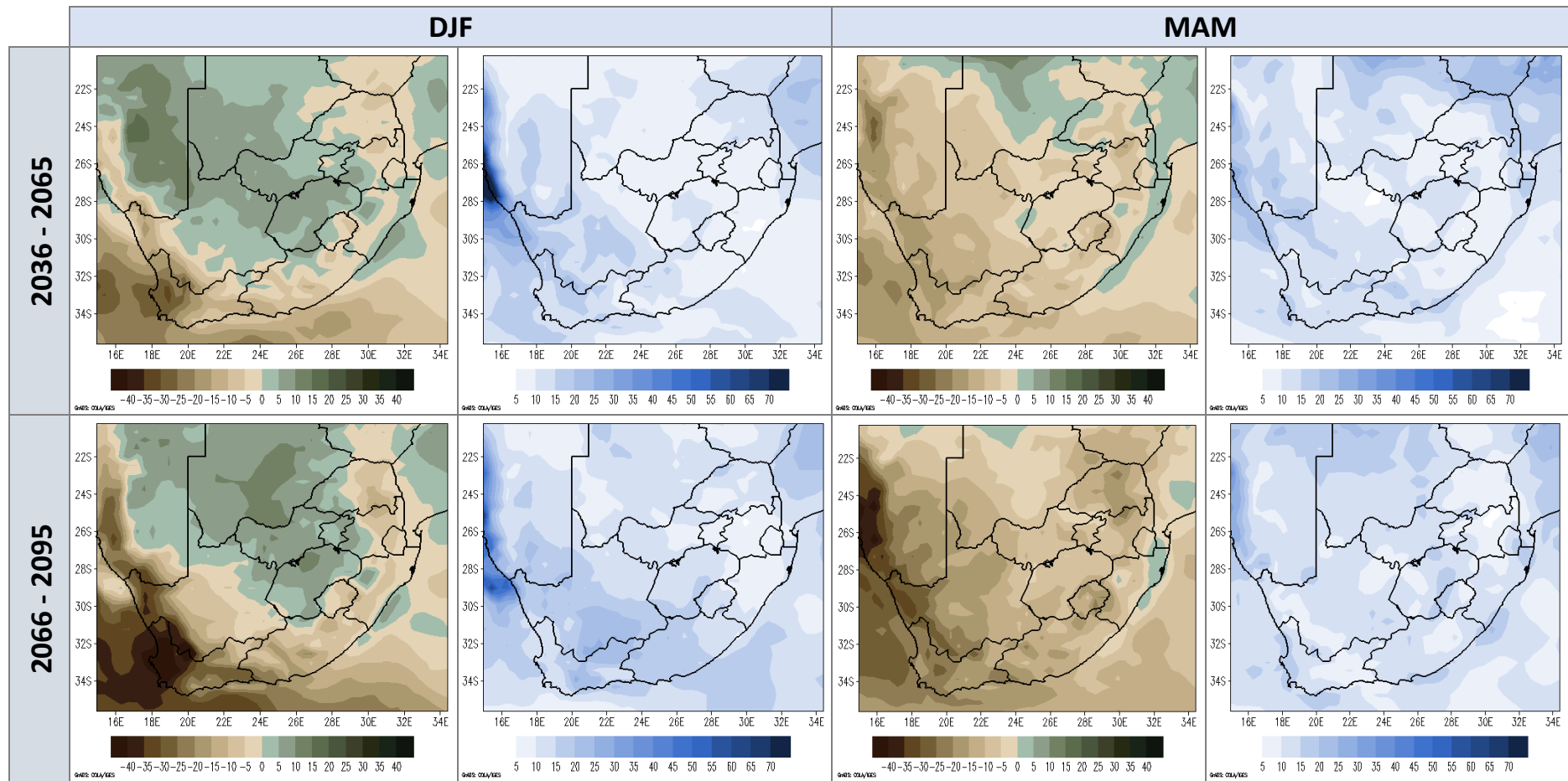

Figure 29: Seasonal total rainfall percentage (%) change (1st and 3rd columns) for the seasons DJF (left) and MAM (right) from the median projected for 2036-2065 (top) and 2066-2095 (bottom), relative to present (1976-2005), under conditions of the RCP 8.5 pathway. The corresponding root-mean-square difference (rmsd) in percentage (%) between the nine ensemble member change anomalies is indicated in the 2nd and 4th columns.

RCP 8.5: Seasonal percentage (%) change in total rainfall - relative to 1975-2005
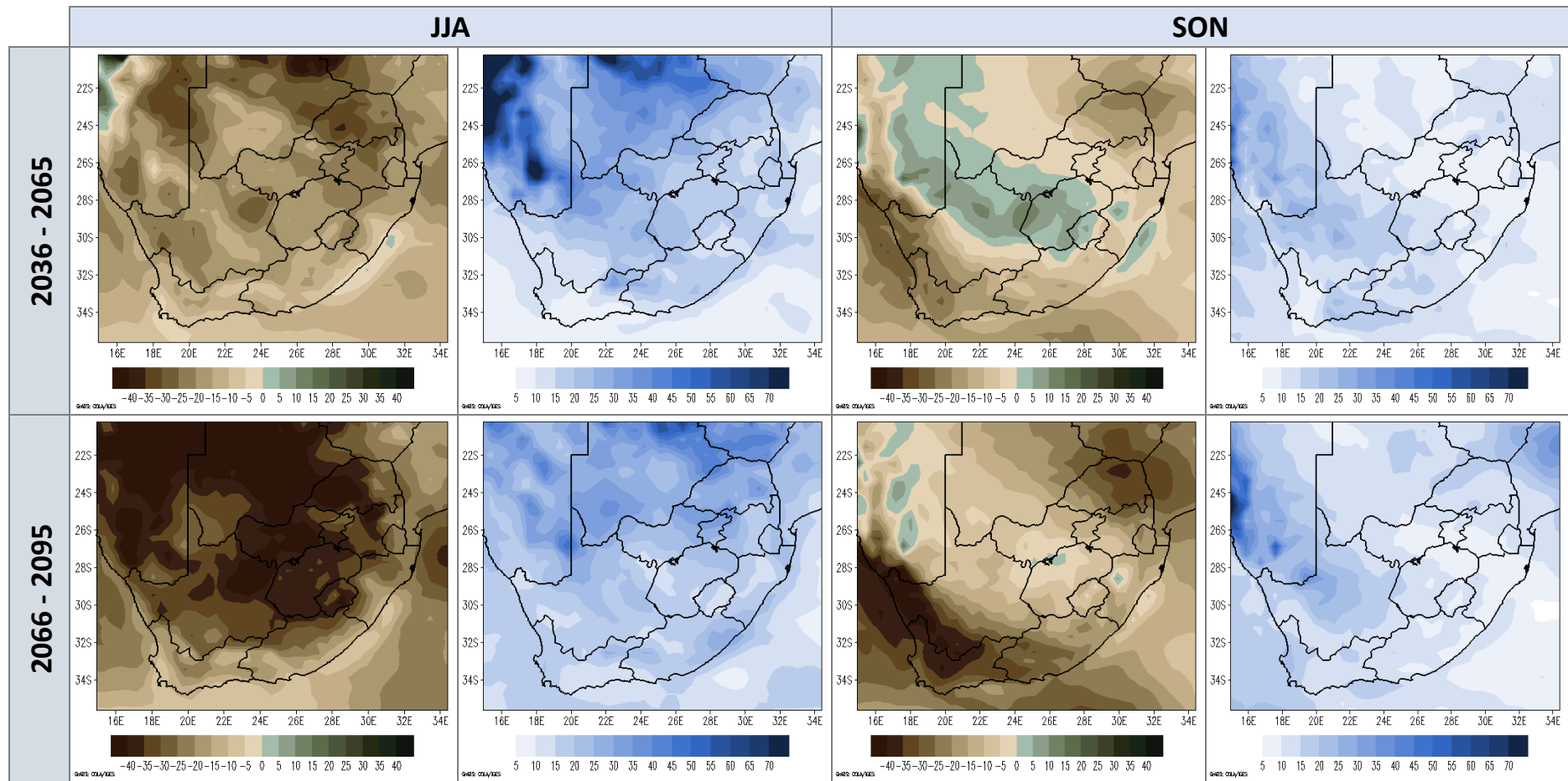

Figure 30: Seasonal total rainfall percentage (%) change (1st and 3rd columns) for the seasons JJA (left) and SON (right) from the median projected for 2036-2065 (top) and 2066-2095 (bottom), relative to present (1976-2005), under conditions of the RCP 8.5 pathway. The corresponding root-mean-square difference (rmsd) in percentage (%) between the nine ensemble member change anomalies is indicated in the 2nd and 4th columns.

8. Acknowledgements

9. Literature references

Arora, V. K., Scinocca, J.F., Boer, G.J., Christian, J.R., Denman, K.L., Flato, G.M., Kharin V.V., Lee, W.G. and Merryfield, W.J. (2011) Carbon emission limits required to satisfy future representative concentration pathways of greenhouse gases. *Geophysical Research Letters*, 38(5), L05805, DOI: 10.1029/2010GL046270.

Collins, W. J., Bellouin, N., Doutriaux-Boucher, M., Gedney, N., Halloran, P., Hinton, T., Hughes, J., Jones, C.D., Joshi, M., Liddicoat, S., Martin, G., O'Connor, F., Rae, J., Senior, C., Sitch, S., Totterdell, I., Wiltshire, A. and Woodward, S. (2011) Development and evaluation of an Earth-system model— HadGEM2. *Geosci. Model Dev*. *Discuss*., 4, 997–1062, DOI: 10.5194/gmd-4-1051-2011

Dunne, J. P., John, J.G., Adcroft, A.J., Griffies, S.M., Hallberg, R.W., Shevliakova, E., Stouffer, R.J., Cooke, W., Dunne, K.A., Harrison, M.J., Krasting, J.P., Malyshev, S.L., Milly, P.C.D., Phillipps, P.J., Sentman, L.T., Samuels, B.L., Spelman, M.J., Winton, M., Wittenbarg, A.T. and Zadeh, N. (2012) GFDL's ESM2 Global Coupled Climate-Carbon Earth System Models. Part I: Physical Formulation and Baseline Simulation Characteristics, *Journal of Climate*, 25(19), 6646-6665.

Fan, Y. and van den Dool, H. (2008) A global monthly land surface air temperature analysis for 1984-present. *J. Geophys. Res*., 113, DOI: 10.1029/2007JD008470.

Giorgi, F. and Mearns, L.O. (2002) Calculation of Average, Uncertainty Range, and Reliability of Regional Climate Change from AOGCM Simulations via the "Reliability Ensemble Averaging" (REA) Method. *J. Climate,* 15, 1141–1158.

Hourdin, F., Foujols, M. A., Codron, F., Guemas, V., Dufresne, J. L., Bony, S., Denvil, Sebastien, Guez, L., Lott, F., Ghattas, J., Braconnot, P., Marti, O., Meurdesoif, Y. and Bopp, L. (2013) Impact of the LMDZ atmospheric grid configuration on the climate and sensitivity of the IPSL-CM5A coupled model. *Clim. Dyn.,* 40, DOI: 10.1007/s00382-012-1411-3, 2167–2192.

Ilyina, T., Six, K.D., Segschneider, J., Maier-Reimer, E., Li, H., and Nuńez-Riboni, I. (2013) The global ocean biogeochemistry model HAMOCC: Model architecture and performance as component of the MPI-Earth System Model in different CMIP5 experimental realizations, *J. Adv. Model. Earth Syst*., DOI:10.002/jame.20017.

IPCC (2013) Climate Change 2013: The Physical Science Basis. Contribution of Working Group I to the Fifth Assessment Report of the Intergovernmental Panel on Climate Change [Stocker, T.F., D. Qin, G.-K. Plattner, M. Tignor, S.K. Allen, J. Boschung, A. Nauels, Y Xia, V. Bex and P.M. Midgley (eds.)]. Cambridge University Press, Cambridge, United Kingdom and New York, NY, USA, 1535 pp.

Jones, C., Giorgi, F. and Asrar G. (2011) The Coordinated Regional Downscaling Experiment (CORDEX). An international downscaling link to CMIP5. Clivar Exchanges 16, 34–40.

Riahi, K., Roa, S., Krey, V., Cho, C., Chirkov, V., Fisher, G., Kindermann, G., Nakicenovic, N and Rafaj, P. (2011) RCP 8.5 – A scenario of comparatively high greenhouse gas emissions. *Climate Change*, 109, 33-57.

Rotstayn, L. D., Collier, M.A., Jeffrey, S.J., Kidston, J., Syktus, J.I., and Wong, K.K. (2013) Anthropogenic effects on the subtropical jet in the Southern Hemisphere: aerosols versus long-lived greenhouse gases. *Environ. Res. Lett.*, 8, DOI: 10.1088/17489326/8/1/014030.

Schneider, U., Becker, A., Finger, P., Meyer-Christoffer, A., Rudolf, B. and Ziese, M. (2011): GPCC Full Data Reanalysis Version 6.0 at 0.5°: Monthly Land-Surface Precipitation from Rain-Gauges built on GTS-based and Historic Data. DOI: 10.5676/DWD GPCC/FD M V7 050.

Rotstayn, L. D., Collier, M.A., Jeffrey, S.J., Kidston, J., Syktus, J.I. and Wong, K.K. (2013) Anthropogenic effects on the subtropical jet in the Southern Hemisphere: aerosols versus long-lived greenhouse gases. *Environ. Res. Lett.*, 8, 014030, DOI: 10.1088/17489326/8/1/014030.

Taylor, K.E., Stouffer, R.J. and Meehl, G.A. (2012) An Overview of CMIP5 and the experimental design. *Bull. Amer. Meteor. Soc.*, 93, 485-498.

Tjiputra, J. F., Roelandt, C., Bentsen, M., Lawrence, D. M., Lorentzen, T., Schwinger, J., Seland, Ø. and Heinze, C. (2013) Evaluation of the carbon cycle components in the Norwegian Earth System Model (NorESM), *Geosci. Model Dev.*, 6, DOI: 10.5194/gmd-6-301-2013, 301-325.

Undén, P., Rontu, L., Jarvinen, H., Lynch, P., Calvo, J., Cats, G., Cuxart, J., Eerola, K., Fortelius, C., Garcia-Moya, J.A., Jones, C., Lenderlink, G., McDonald, A., McGrath, R., Navascues, B., Nielsen, N.W., Odegaard, V., Rodriguez, E., Rummukainen, M., Room, R., Sattler, K., Sass, B.H, Savijarvi, H., Schreur, B.W., Sigg, R., The, H. and Tijm, A. (2002) *HIRLAM-5 Scienti_c Documentation*, HIRLAM-5 Project, c/o Per Unden SMHI, S-601 76 Norrkoping, Sweden, 146pp.

Voldoire, A., Sanchez-Gomez, E., Salas y Mélia, D., Decharme, B., Cassou, C., Sénési, S., Valcke, S., Beau, I., Alias, A., Chevallier, M., Déqué, M., Deshayes, J., Douville, H., Fernandez, E., Madec, G., Maisonnave, E., Moine, M.P., Planton, S., Saint-Martin, D., Szopa, S., Tyteca, S., Alkama, R., Belamari, S., Braun, A., Coquart, L. and Chauvin, F. (2013) The CNRM-CM5.1 global climate model: Description and basic evaluation. *Climate Dyn.*, 40, DOI:10.1007/s00382-011-1259-y, 2091–2121.

Watanabe, S., Hajima,T., Sudo, K., Nagashima, T., Takemura, T., Okajima, H., Nozawa, T., Kawase, H., Abe, M., Yokohata, T., Ise, T., Sato, H., Kato, E., Takata, K., Emori, S. and Kawamiya, M. (2011) MIROC-ESM 2010: Model description and basic results of CMIP5-20c3m experiments. *Geosci. Model Dev.*, 4, DOI: 10.5194/gmd-4-845-2011, 845–872.

Web site links:

CORDEX
http://www.cordex.org/

DEA (2011) National Climate Change Response White Paper:
https://www.environment.gov.za/sites/default/files/legislations/national_climatechange_response_whitepaper.pdf

IPCC (2013):
https://www.ipcc.ch

WCRP:

https://www.wcrp-climate.org/